bioRxiv preprint doi: https://doi.org/10.1101/190298; this version posted October 25, 2018. The copyright holder for this preprint (which was not certified by peer review) is the author/funder, who has granted bioRxiv a license to display the preprint in perpetuity. It is made available under aCC-BY-NC-ND 4.0 International license.

Precise excitation-inhibition balance controls gain and timing in the hippocampus

Aanchal Bhatia[1], Sahil Moza[1], Upinder S. Bhalla[2]

National Centre for Biological Sciences, Tata Institute of Fundamental Research, Bellary Road, Bangalore 560065 India

[1]These authors contributed equally

[2]Lead Contact (bhalla@ncbs.res.in)

ABSTRACT

Excitation-inhibition (EI) balance controls excitability, dynamic range, and input gating in many brain circuits. Subsets of synaptic input can be selected or 'gated' by precise modulation of finely tuned EI balance, but assessing the granularity of EI balance requires combinatorial analysis of excitatory and inhibitory inputs. Using patterned optogenetic stimulation of hippocampal CA3 neurons, we show that hundreds of unique CA3 input combinations recruit excitation and inhibition with a nearly identical ratio, demonstrating precise EI balance at the hippocampus. Crucially, the delay between excitation and inhibition decreases as excitatory input increases from a few synapses to tens of synapses. This creates a dynamic millisecond-range window for postsynaptic excitation, controlling membrane depolarization amplitude and timing via subthreshold divisive normalization. We suggest that this combination of precise EI

bioRxiv preprint doi: https://doi.org/10.1101/190298; this version posted October 25, 2018. The copyright holder for this preprint (which was not certified by peer review) is the author/funder, who has granted bioRxiv a license to display the preprint in perpetuity. It is made available under aCC-BY-NC-ND 4.0 International license.

balance and dynamic EI delays forms a general mechanism for millisecond-range input gating and subthreshold gain control in feedforward networks.

INTRODUCTION

Individual neurons in the brain can receive tens of thousands of excitatory (E) and inhibitory (I) synaptic inputs. Under normal conditions, the ratio of excitatory to inhibitory input remains invariant, a robust property of the nervous system, termed EI balance(Anderson, Carandini, & Ferster, 2000; Atallah & Scanziani, 2009; Okun & Lampl, 2008, 2009; Wehr & Zador, 2003). Disruption of balance is linked with several pathologies, including epilepsy, autism spectrum disorders and schizophrenia(Yizhar et al., 2011).

Theoretically, neurons in 'detailed balanced' EI networks receive balanced responses from all subsets of presynaptic inputs(Tim P Vogels & Abbott, 2009), and neurons in 'tightly balanced' EI networks receive inputs balanced at fast (<10 ms) timescales(Denève & Machens, 2016). Together, these properties constitute a 'precisely balanced' network(Hennequin, Agnes, & Vogels, 2017). This precise balance on all synaptic subsets can be exploited by the brain for 'input gating'. In this process, neurons can be driven by selective shifts in EI ratios at specific inputs, while other inputs remain balanced in the background. This constitutes a flexible and instantaneous information channel local to the shifted synapses(Kremkow, Aertsen, & Kumar, 2010; Tim P Vogels & Abbott, 2009).

Our current understanding of EI balance is based on measurements made at single neurons in response to various stimuli. Strong EI correlations have been seen in response to series of tones in auditory cortex(Wehr & Zador, 2003; Zhang, Tan, Schreiner, & Merzenich, 2003; Zhou et al., 2014), whisker stimulation in somatosensory cortex(Wilent & Contreras, 2005), during cortical up states *in vitro*(Shu, Hasenstaub, Badoual, Bal, & McCormick, 2003) and *in vivo*(Haider, Duque, Hasenstaub, & McCormick, 2006), during gamma oscillations *in vitro* and *in*

bioRxiv preprint doi: https://doi.org/10.1101/190298; this version posted October 25, 2018. The copyright holder for this preprint (which was not certified by peer review) is the author/funder, who has granted bioRxiv a license to display the preprint in perpetuity. It is made available under aCC-BY-NC-ND 4.0 International license.

vivo(Atallah & Scanziani, 2009), and during spontaneous activity(Okun & Lampl, 2008). At the synaptic scale, the ratio of excitatory and inhibitory synapses on various dendrites of a neuron has been shown to be conserved (Iascone et al., 2018)However, the precision and presynaptic origin of balance is not well understood. It remains to be established if EI balance arises transiently from complex temporal dynamics of several presynaptic layers, if it requires summation of inputs from multiple presynaptic populations, or if it exists even at subsets of a single presynaptic population. This granularity of EI balance, of both presynaptic identity and number of inputs, can determine the precision with which synaptic inputs can be selected or 'independently gated' to affect postsynaptic activity.

In this study we address two key open questions in the field. First, can EI balance arise even in a single layer feedforward network, and if so, at what granularity of network subsets do postsynaptic cells experience balanced excitation and inhibition? Second, how do excitation and inhibition integrate to encode and communicate information at the postsynaptic neuron? We addressed these questions *in vitro*, to isolate the hippocampal network from background activity, and to deliver precisely controlled combinatorial stimuli. We stimulated channelrhodopsin-2 (ChR2) expressing CA3 neurons in several combinations using optical patterns, and measured responses in CA1.

We report that hundreds of randomly chosen subsets of CA3 neurons provide excitatory and feedforward inhibitory inputs to CA1 cells with a close to identical ratio, demonstrating for the first time, precise balance(Hennequin et al., 2017) in the brain. On examining the integration of excitation and feedforward inhibition, we found that it leads to divisive normalization at subthreshold potentials. Subthreshold Divisive Normalization (SDN) operates by preserving the amplitude of the small excitatory inputs in a manner independent of inhibition, and for larger inputs, it uses balanced inhibition to progressively reduce the output with increasing input. This novel gain control operation encodes input information in both amplitude and timing of the CA1 response.

bioRxiv preprint doi: https://doi.org/10.1101/190298; this version posted October 25, 2018. The copyright holder for this preprint (which was not certified by peer review) is the author/funder, who has granted bioRxiv a license to display the preprint in perpetuity. It is made available under aCC-BY-NC-ND 4.0 International license.

RESULTS

Optical stimuli at CA3 elicit subthreshold responses at CA1

To provide a wide range of non-overlapping stimuli, we projected patterned optical stimuli onto channelrhodopsin-2 (ChR2) expressing CA3 neurons in acute hippocampal slices. We used CA3-cre mice to achieve CA3-specific localization of ChR2 upon injection of a Lox-ChR2 virus (**Fig. 1a, Methods**). We used a Digital Micromirror Device (DMD) projector (**Methods**, **Supplementary Fig. S1**) to generate spatiotemporal optical patterns in the form of a grid of several 16um x 16um squares, each square approximating the size of a CA3 soma(N Ishizuka, Cowan, & Amaral, 1995) (**Fig. 1d**). This grid was centered at the CA3 cell body layer, and extended to the dendritic layer (**Fig. 1a**). Each optical pattern consisted of 1 to 9 such randomly chosen grid squares, presented to CA3 cells as stimulus, at an inter-stimulus interval of 3 seconds (**Fig. 1a, 1d**, **Methods**). In a typical experiment, several randomly chosen stimulus patterns with different number of input squares were delivered to CA3, in 3 successive repeats. We first characterized how CA3 responded to the grid stimulation (**Fig. 1b,e,f,g**). CA3 neurons fired reliably with a <2ms jitter, calculated as the standard deviation of the time of first spike (**Fig. 1f**) (n = 8 CA3 cells, inputs = 52, median = 0.44ms, N = 1 to 9 squares). No desensitization occurred during the timeframe of an experiment, and the probability of spiking remained constant between the 3 repeats (**Fig. 1g**) (n = 7 CA3 cells, N = 1 to 9 squares). Thus, we could stimulate CA3 with hundreds of distinct optical stimuli in each experiment.

We then recorded postsynaptic potentials (PSPs) evoked at patched CA1 neurons while optically stimulating CA3 cells (**Fig. 1c,h,i,j**). A wide range of stimulus positions in CA3 excited CA1 neurons (**Fig. 1c**). Stimulation of CA3 elicited excitation and feedforward inhibition at CA1 (**Fig. 1a**, **Supplementary Fig.S3**). Most stimuli elicited subthreshold responses (N = 1 to 9 squares). Action potentials occurred in only 0.98% of trials (183 out of 18,668 trials, n = 38 cells,

bioRxiv preprint doi: https://doi.org/10.1101/190298; this version posted October 25, 2018. The copyright holder for this preprint (which was not certified by peer review) is the author/funder, who has granted bioRxiv a license to display the preprint in perpetuity. It is made available under aCC-BY-NC-ND 4.0 International license.

N = 1 to 9 squares). This helped rule out any significant feedback inhibition from CA1 interneurons for all our experiments. Restriction of ChR2 to CA3 pyramidal cells, coupled with the fact that ~99% of all recorded CA1 responses were subthreshold, ensured that the recorded inhibition was largely feedforward (disynaptic)(**Fig. 1a**). Responses to the same 1-square stimulus were consistent, 84.74% responses showed less than 0.5 variance by mean (695 stimuli, 3 repeats each, n = 28 cells, N = 1 square) (**Fig. 1i**). Notably, the distribution of all 1 square responses had a mode at 0.25 mV, which is close to previous reports of a 0.2mV somatic response of single synapses in CA1 neurons(Magee & Cook, 2000)(8845 trials, n = 38 cells, N = 1 square) (**Fig. 1j**).

bioRxiv preprint doi: https://doi.org/10.1101/190298; this version posted October 25, 2018. The copyright holder for this preprint (which was not certified by peer review) is the author/funder, who has granted bioRxiv a license to display the preprint in perpetuity. It is made available under aCC-BY-NC-ND 4.0 International license.

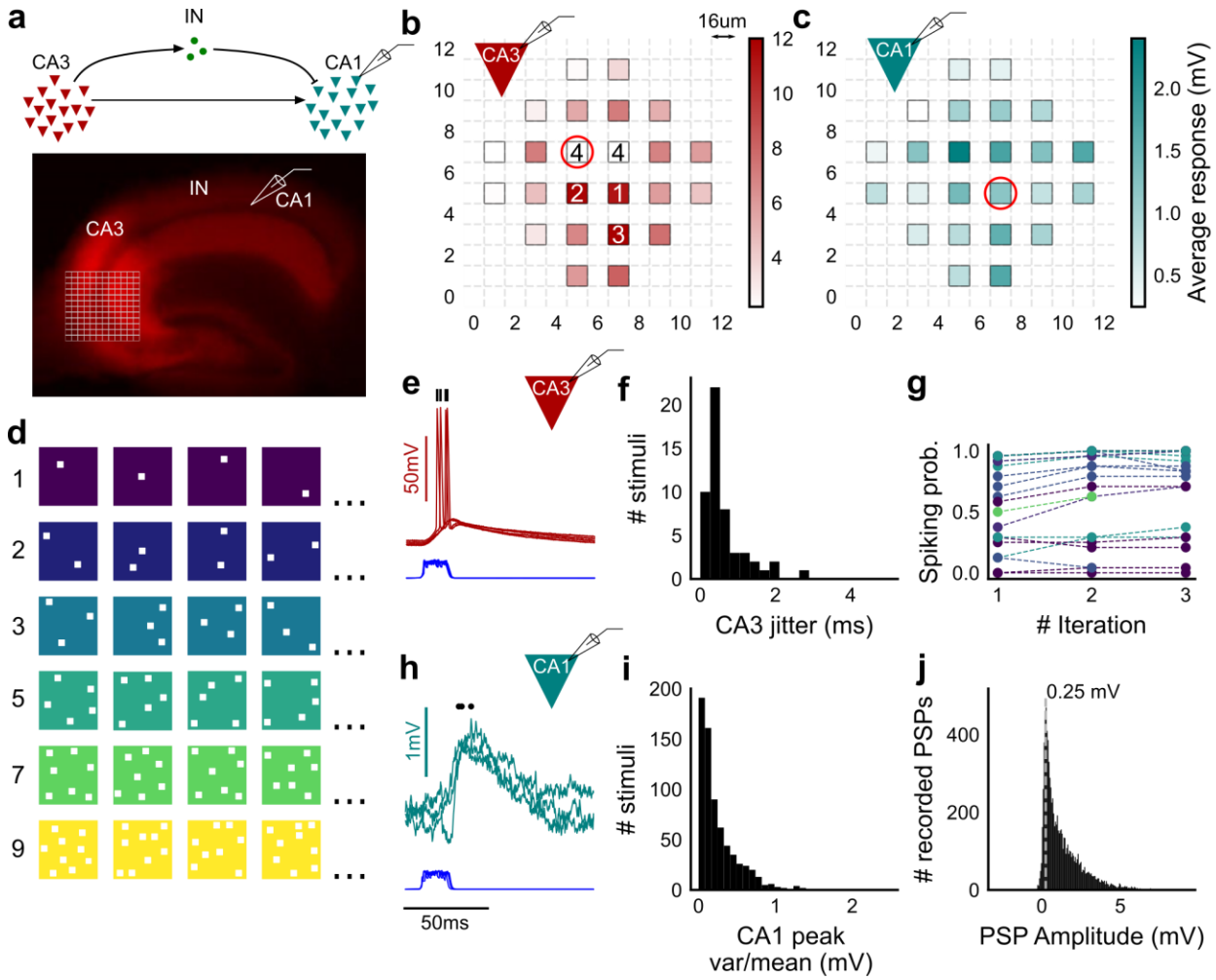

Figure 1: Stimulating CA3-CA1 network with hundreds of optical patterns

(**a**) Top, schematic of the CA3-CA1 circuit with direct excitation and feedforward inhibition. Bottom, image of a hippocampus slice expressing ChR2-tdTomato (red) in CA3 in a Cre-dependent manner. Optical stimulation grid (not drawn to scale) was centered at the CA3 cell body layer and CA1 neurons were patched.

(**b**) Heat map of CA3 neuron responses with 1 grid square active at a time. A CA3 neuron was patched and optically stimulated, in random spatio-temporal order, on the grid locations marked with gray border. This cell spiked in response to 5 stimuli (marked with number inside representing spike counts over 4 trials) out of 24 such 1 square stimuli delivered. Color in grid squares represents peak V_m change from

bioRxiv preprint doi: https://doi.org/10.1101/190298; this version posted October 25, 2018. The copyright holder for this preprint (which was not certified by peer review) is the author/funder, who has granted bioRxiv a license to display the preprint in perpetuity. It is made available under aCC-BY-NC-ND 4.0 International license.

baseline, averaged over trials when the neuron did not spike. Locations where the cell spiked all 4 times are in white.

(**c**) Heatmap of CA1 responses while CA3 neurons were stimulated with 1 square optical stimuli. Colormap represents peak V_m, change averaged over 3 repeats.

(**d**) Schematic of patterned optical stimuli. Examples of combinations of N-square stimuli where N could be 1, 2, 3, 5, 7 or 9 (in rows).

(**e**) Spikes in response to 4 repeats for the circled square, in **b**. Spike times are marked with a black tick, showing variability in evoked peak times. Blue trace at the bottom represents photodiode measurement of the stimulus duration. Scale bar for time, same as **h**.

(**f**) Distribution of jitter in spike timing (SD) for all stimuli for all CA3 cells (n = 8 cells).

(**g**) CA3 spiking probability (fraction of times a neuron spiked across 24 stimuli, repeated thrice) is consistent over a single recording session. Randomization of the stimulus pattern prevented ChR2 desensitization. Circles, colored as in **d,** depict spiking probability on each repeat of a stimulus set with connecting lines tracking 3 repeats of the set (n = 7 cells).

(**h**) PSPs in response to 3 repeats of the circled square in **c**. Peak times are marked with an asterisk. Blue photodiode trace same as (**e**).

(**i**) Distribution of peak PSP amplitude variability (variance/mean) for all 1-square responses. (n = 28 cells, stimuli = 695)

(**j**) Histogram of peak amplitudes of all PSPs elicited by all 1-square stimuli, over all CA1 cells. Gray dotted line marks the mode (n = 38 cells, trials = 8845).

Arbitrarily chosen CA3 inputs show precise EI balanced at CA1

To examine the relationship between excitation and inhibition, we voltage clamped CA1 neurons, first at the inhibitory (-70 mV) and then at the excitatory (0 mV) reversal potential to record Excitatory and Inhibitory Post Synaptic Currents (EPSCs and IPSCs) respectively. We first presented 5 different patterns of 5 squares each, at both of these potentials, and recorded EPSCs and IPSCs. We found strong proportionality between excitation and inhibition for every stimulus pattern (**Fig. 1d, 2a, b, c**). This suggested that inputs from even random groups of CA3 neurons may be balanced at CA1. Repeats with the same stimulus pattern gave consistent responses, but different patterns evoked different responses (**Fig. 2a, Supplementary Fig. S3b**). This indicated that the optically-driven stimuli were able to reliably activate different

bioRxiv preprint doi: https://doi.org/10.1101/190298; this version posted October 25, 2018. The copyright holder for this preprint (which was not certified by peer review) is the author/funder, who has granted bioRxiv a license to display the preprint in perpetuity. It is made available under aCC-BY-NC-ND 4.0 International license.

subsets of synaptic inputs on the target neuron. Next, we asked, in what range of input strengths does random input yield balance? We presented 5 different patterns for each of 1, 2, 3, 5, 7 or 9 square combinations at both recording potentials. Surprisingly, all stimuli to a cell elicited excitatory and inhibitory responses in the same ratio, irrespective of response amplitude (**Fig. 2b, c**) (n =13 CA1 cells, area under curve, mean R^2 = 0.89+/- 0.06 SD, **Supplementary Fig.S2**). Notably, the mode of single-square responses was ~0.25 mV, close to single synapse PSP estimates(Magee & Cook, 2000) (**Fig. 1j**). However, given the low synaptic release probabilities at the CA3-CA1 synapse (~0.2(Murthy, Sejnowski, & Stevens, 1997)), we estimate that the granularity of the balance may be of the order of 5-10 synapses (**Supplementary Fig. S3 d, e**) synapses. The slope of the regression line through all stimulus-averaged responses for a CA1 cell was used to calculate the Inhibition/Excitation (I/E) ratio for the cell. IPSC/EPSC ratio will be here onwards referred to as I/E ratio, unless mentioned otherwise. This I/E ratio was typically between 2 and 5 (**Fig. 2d**).The variability of I/E ratios over all stimuli for a cell was lower than the variability of all stimuli across cells (for 12 out of 13 cells, **Supplementary Fig. S3c**). The high R^2 values for all cells showed tight proportionality for all stimuli (**Fig. 2e**). The residual distribution remained symmetric for increasing numbers of spots, again showing that they were not affected by the number of stimulus squares presented (**Supplementary Fig. S3a**).While feedforward inhibition is expected to increase with excitation, convergence of I/E ratios for randomly chosen inputs to a cell to a single number was unexpected, since shared interneurons consist of only about 10% of the total neuronal population (Woodson, 1989; Bezaire and Soltesz, 2013).

We next tested the hypothesis that the observed correlation between excitatory and inhibitory inputs was due to an averaged sum over many untuned (globally balanced) synapses, as opposed to tuning in excitatory and inhibitory synaptic weights (detailed balance). To address this, we took three approaches.

bioRxiv preprint doi: https://doi.org/10.1101/190298; this version posted October 25, 2018. The copyright holder for this preprint (which was not certified by peer review) is the author/funder, who has granted bioRxiv a license to display the preprint in perpetuity. It is made available under aCC-BY-NC-ND 4.0 International license.

1. We built a model of excitatory and inhibitory synaptic weights to a neuron with different amounts of weight tuning, parameterized by rho (ρ), which takes values between 0 (no tuning or global balance) and 1 (detailed balance) (**Methods**). For values between 0 and 1, ρ determined the degree of correlation between the basal excitatory and inhibitory synaptic weights. The model assumed proportionality of numbers of EI afferents, which admittedly is a simplification, and might itself require a tuning process to achieve. However, there is some evidence that the proportion of excitatory and inhibitory synapses on hippocampal dendrites is conserved(Liu, 2004). We wanted to see how correlations between excitatory and inhibitory inputs change with weight tuning, even under this stringent condition of number balance. We observed tight correlations between excitatory and inhibitory inputs without weight tuning, but only if the synaptic weight distribution of synapses was narrow. Further, for a narrow weight distribution, the change from global to detailed balance had little effect on EI correlations. In contrast, weight tuning was required to see EI balance for wider synaptic weight distributions, especially for stimuli which activated small numbers of synapses (**Fig. 2g**). We next calculated the width of the smallest responses (1-square GABAzine EPSP) as a proxy for the basal weight distribution (**Supplementary Fig. S4a**). We found that the basal excitatory weight distribution thus obtained necessitates that excitatory and inhibitory synaptic weights be co-tuned to be able to observe EI balance. (marked with arrow in **Fig. 2g**, **Methods**).
2. With the reasoning developed above, we checked for EI balance in the smallest inputs in our datasets - 1 and 2 square data from voltage clamped cells (having 5 or more input patterns per cell) (**Supplementary Fig. S3d**), and only 1 square from current clamped cells (24 inputs per cell) (**Supplementary Fig. S3 e,f**). We found that the responses corresponding to a few synapses per input (**Fig. 1j, Supplementary Fig. S3 d,e,f,i**)

bioRxiv preprint doi: https://doi.org/10.1101/190298; this version posted October 25, 2018. The copyright holder for this preprint (which was not certified by peer review) is the author/funder, who has granted bioRxiv a license to display the preprint in perpetuity. It is made available under aCC-BY-NC-ND 4.0 International license.

were balanced for excitation and inhibition (**Fig. 2f, h**), suggesting tuning of excitation and inhibition.

3. In addition, the model also predicted a tuning dependent change in the correlations of variability of excitation and inhibition for repeats of the same stimulus. For a wide synaptic weight distribution, increase in tuning increased EI variability correlations (**Supplementary Fig. 3h,j**). As with EI mean correlations (**Fig 2 h,i**), weight tuning had little effect on narrow synaptic weight distributions. Again, our calculated synaptic weight distribution was in the range where strong variability correlations would be seen only if synaptic weights were tuned. We found strong correlations between excitatory and inhibitory standard deviations in our voltage-clamp dataset, suggesting that there is detailed balance in the network (**Supplementary Fig. S3g,i**).

Together, these results imply that the hypothesis of proportional increase in EI afferents in a globally balanced network leading to EI correlations is inconsistent with our observations of wide weight distribution and correlated EI amplitude and variability at small input strengths. This supports the existence of weight tuning and hence detailed balance in the CA3-CA1 network.

Overall, we found stimulus-invariant proportionality of excitation and inhibition for any randomly selected input, over a large range of stimulus strengths from a single presynaptic network. In addition to detailed balance, we show below that there is tight balance, i.e., the timing of the balanced feedforward inhibition was within a few milliseconds of the excitation (**Fig 6g, h**). Thus, we concluded that the CA3-CA1 circuit exhibits precise (both detailed and tight) balance(Hennequin et al., 2017).

bioRxiv preprint doi: https://doi.org/10.1101/190298; this version posted October 25, 2018. The copyright holder for this preprint (which was not certified by peer review) is the author/funder, who has granted bioRxiv a license to display the preprint in perpetuity. It is made available under aCC-BY-NC-ND 4.0 International license.

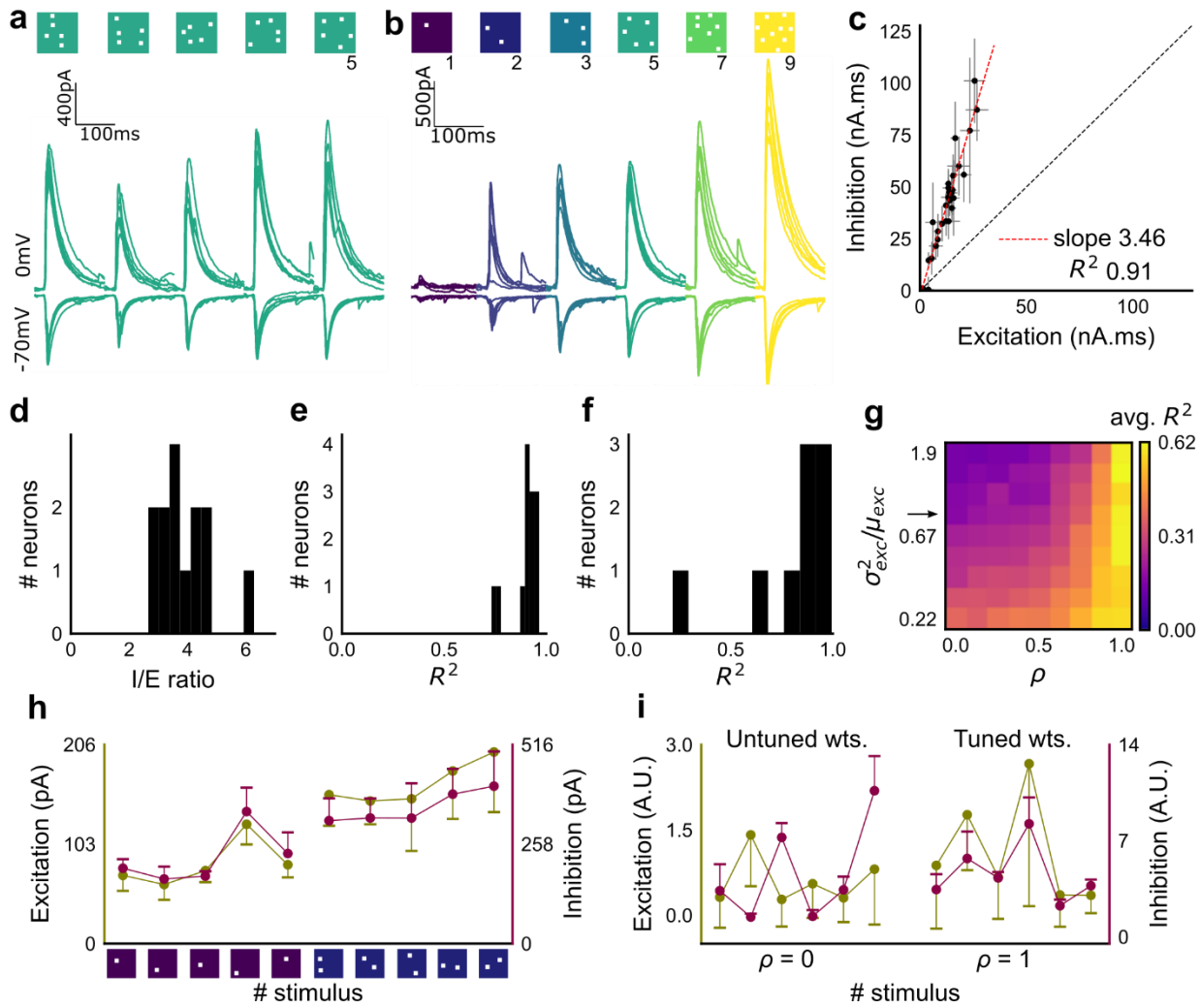

Figure 2: **Excitation and inhibition are tightly balanced for all stimuli to a CA1 cell**

(**a**) Monosynaptic excitatory postsynaptic currents (EPSCs, at -70mV) and disynaptic inhibitory postsynaptic currents (IPSCs, at 0mV) in response to 5 different stimulus combinations of 5 squares each. All combinations show proportional excitatory and inhibitory currents over 6 repeats. Top: schematic of 5 square stimuli.

(**b**) EPSCs and IPSCs are elicited with the same I/E ratio in response to 6 repeats of a combination, and across 6 different stimuli from 1 square to 9 squares, for the same cell as in a. Top, schematic of the stimuli.

(**c**) Area under the curve for EPSC and IPSC responses, obtained by averaging over 6 repeats, plotted against each other for all stimuli to the cell in **a, b**. Error bars are s.d.

(**d**) Summary of I/E ratios for all cells (n = 13 cells).

(**e**) Summary for all cells of R^2 values of linear regression fits through all points. Note that 11 out of 13 cells had R^2 greater than 0.9, implying strong proportionality.

(**f**) Same as **e**, but with linear regression fits for 1 and 2 square responses, showing that even small number of synapses are balanced for excitation and inhibition (n = 9 cells).

bioRxiv preprint doi: https://doi.org/10.1101/190298; this version posted October 25, 2018. The copyright holder for this preprint (which was not certified by peer review) is the author/funder, who has granted bioRxiv a license to display the preprint in perpetuity. It is made available under aCC-BY-NC-ND 4.0 International license.

(**g**) Phase plot from the model showing how tuning of synapses (ρ) affects observation of EI balance (R^2) for various values of variance/mean of the basal weight distribution. Changing the scale of the basal synaptic weight distributions against tuning parameter ρ affects goodness of EI balance fits. Arrow indicates where our observed synaptic weight distribution lay.

(**h**) Example of EI correlations (from data) for 1 and 2 square inputs for an example cell from **f**. Bottom, schematic of the stimuli. Excitation and inhibition are colored olive and purple respectively. Error bars are s.d.

(**i**) Examples of EI correlation (from model) for small number of synapses, from the row marked with arrow in **g**. The left and right curves show low and high correlations when EI synapses are untuned (ρ = 0) and tuned respectively (ρ = 1) (A.U. = Arbitrary Units) .Colors, same as **h**. Error bars are s.d.

Combinatorial CA3 inputs sum sublinearly at CA1

We next asked how CA3 inputs, that lead to balanced excitatory and feedforward inhibitory conductances, transform into membrane potential change at CA1 neurons. Based on anatomical studies, CA3 projections are likely to arrive in a distributed manner over a wide region of the dendritic tree of CA1 pyramidal neuron(Norio Ishizuka, Weber, & Amaral, 1990)(**Fig. 3a**). While pairwise summation at CA1 has been shown to be largely linear in absence of inhibition(Cash & Yuste, 1999), the degree of heterogeneity of summation in response to spatially distributed excitatory and inhibitory synaptic inputs is not well understood (except, see Lovett-Barron, et al., 2012(Lovett-Barron et al., 2012)). To avoid biases that may arise from a single response measure during input integration(Poirazi, Brannon, & Mel, 2003), we examined PSPs using four different measures (**Fig. 3c**). These were peak amplitude, area under curve (AUC), average membrane potential and area under curve till peak (**Fig. 3c**).

We looked at input integration by presenting stimulus sets of 5 input squares to a given cell, with each stimulus set ranging from 24 to 225 combinations of inputs. We initially tested the center of our range of 1-9 squares (5-square inputs) before expanding the dataset to the full

bioRxiv preprint doi: https://doi.org/10.1101/190298; this version posted October 25, 2018. The copyright holder for this preprint (which was not certified by peer review) is the author/funder, who has granted bioRxiv a license to display the preprint in perpetuity. It is made available under aCC-BY-NC-ND 4.0 International license.

range (Figure 4).We also recorded the responses to all squares of the grid individually (1 square input). The 1 square PSP peak response amplitude with inhibition intact (control) was not distinguishable from that with inhibition blocked (GABAzine) (**Methods**, **Supplementary Fig. S4a**). As analyzed below (**Figure 6**), we find that the apparent lack of effect of GABAzine for very small inputs is because inhibition arrives with a delay that does not affect the peak response of the neuron. The 'observed' response for a given square combination was plotted against the 'expected' response, obtained by linearly summing responses of the individual squares constituting that combination (**Fig. 3b, d**). Perfectly linear summation would imply that a multi-square combination of inputs would elicit the same response as the sum of the responses to the individual squares (dotted line, **Fig. 3d**). **Figure 3e** shows responses of a single cell stimulated with 126 distinct 5-square combinations. The 'observed' response was sublinear as compared to the 'expected' summed response, for most stimuli (**Fig. 3e**). For all the four measures in **3c**, CA3 inputs summed sublinearly at CA1 (**Fig. 3e, Supplementary Fig.S4c**). At this point, we hypothesised that the observed sublinearity might mostly be due to inhibition divisively scaling excitation, since excitatory and inhibitory conductances were proportional for all stimuli (**Fig. 2**). We later tested this hypothesis by blocking inhibition (**Figure 5**). For all responses measured over all cells, 93.35% responses were individually sublinear, with distribution having mean 0.57± 0.31 (SD) (**Fig. 3f**, **Supplementary Fig. S4 d**). The slope of the regression line, which indicated the extent of sublinearity, varied between cells, with mean 0.38 ± 0.22 (SD) (n = 33 cells) (**Fig. 3g**).

Thus, we found that the CA3-CA1 network exhibits sublinear summation over a large number of inputs.

bioRxiv preprint doi: https://doi.org/10.1101/190298; this version posted October 25, 2018. The copyright holder for this preprint (which was not certified by peer review) is the author/funder, who has granted bioRxiv a license to display the preprint in perpetuity. It is made available under aCC-BY-NC-ND 4.0 International license.

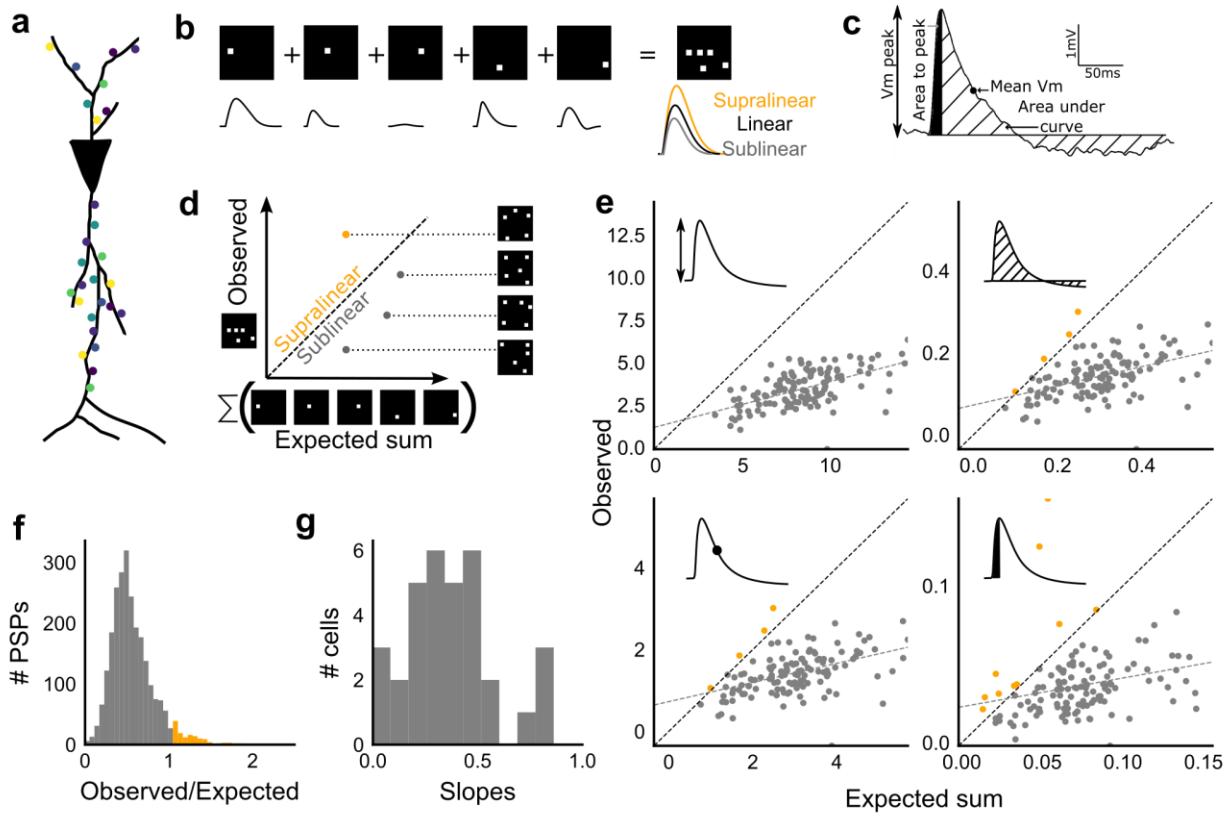

Figure 3: **Excitatory and feed-forward inhibitory inputs from CA3 integrate sublinearly at CA1**

(**a**) Schematic of a neuron receiving synaptic input distributed over its dendritic tree.

(**b**) Schematic of input integration. Top, five 1-square stimuli presented individually, and a single 5-square stimulus comprising of the same squares. Bottom, PSPs elicited as a response to these stimuli. 5-square PSP can be larger (supralinear, orange), equal to (linear, black), or smaller (sublinear, gray) than the sum of the single square PSPs.

(**c**) A PSP trace marked with the 4 measures used for further calculations. PSP peak, PSP area, area to peak and mean voltage are indicated.

(**d**) Schematic of the input integration plot. Each circle represents response to one stimulus combination. 'Observed' (true response of 5 square stimulation) on Y-axis and 'Expected' (linear sum of 1 square responses) is on X-axis.

(**e**) Most responses for a given cell show sublinear summation for a 5-square stimulus. The 4 panels show sublinear responses for 4 different measures (mentioned in **c**) for the same cell. The grey dotted line is the regression line and the slope of the line is the scaling factor for the responses for that cell. For peak (mV), area (mV.ms), average (mV), and area to peak (mV.ms); slope = 0.27, 0.23, 0.23, 0.18; R^2 0.57,

bioRxiv preprint doi: https://doi.org/10.1101/190298; this version posted October 25, 2018. The copyright holder for this preprint (which was not certified by peer review) is the author/funder, who has granted bioRxiv a license to display the preprint in perpetuity. It is made available under aCC-BY-NC-ND 4.0 International license.

0.46, 0.46, 0.26 respectively. The responses to AUC and average are similar because of the similarity in the nature of the measure.

(**f**) Distribution of Observed/Expected ratio of peaks of all responses for all 5-square stimuli (mean= 0.57, SD = 0.31), from all recorded cells pooled. 93.35% responses to 5-square stimuli were sublinear (2513 PSPs, n = 33 cells).

(**g**) Distribution of slopes for peak amplitude of 5-square stimuli (mean = 0.38, SD =0.22). Regression lines for all cells show that all cells display sublinear (<1 slope) summation (n = 33 cells).

CA3-CA1 network performs Subthreshold Divisive Normalization

We then tested how summation sublinearity scaled with a larger range of inputs. We noted that nonlinear functions can be observed better with a large range of inputs(Poirazi et al., 2003), and therefore increased the stimulus range (**Supplementary Fig. S5**).GABAergic inhibition has been shown to be responsible for sublinear summation when Schaffer collateral and perforant path inputs are delivered simultaneously to CA1(Enoki, Inoue, Hashimoto, Kudo, & Miyakawa, 2001).We hypothesized that the sublinearity within the CA3-CA1 network might also occur due to the effect of inhibition. In general, inhibition may interact with excitation to perform arithmetic operations like subtraction, division, and normalization(Carandini & Heeger, 2012). In order to predict the operation performed by EI integration at the CA3-CA1 network, we created a composite model to fit and test for the above three possibilities: subtractive inhibition, divisive inhibition, and divisive normalization (**equation (1)**). **Equation (1)** describes how inhibition controls the 'observed' response ($\boldsymbol{\theta}$) as a function of 'expected' response ($\boldsymbol{\varepsilon}$), for the

bioRxiv preprint doi: https://doi.org/10.1101/190298; this version posted October 25, 2018. The copyright holder for this preprint (which was not certified by peer review) is the author/funder, who has granted bioRxiv a license to display the preprint in perpetuity. It is made available under aCC-BY-NC-ND 4.0 International license.

above three operations. Alpha (α) can be thought to be a subtractive inhibition parameter, beta (β) as a divisive inhibition parameter, and gamma (γ) a normalization parameter (**Fig. 4a**).

$$\boldsymbol{\theta} = \boldsymbol{\varepsilon} - \frac{\beta\boldsymbol{\varepsilon}}{\gamma + \boldsymbol{\varepsilon}}\boldsymbol{\varepsilon} - \alpha \qquad (\mathbf{1})$$

Using the framework of **equation (1)**, we asked what computation was performed at the CA3-CA1 network. We recorded from CA1 cells while stimulating CA3 with many combinations of 2, 3, 5, 7 or 9 squares (**Fig. 4b**). We selected cells with at least 50 input combinations, and pooled responses from all stimuli to a cell. Then, we fit **equation (1)** to the PSP amplitudes (**Fig. 4b**). From visual inspection, the subtractive inhibition model, $\boldsymbol{\theta} = \boldsymbol{\varepsilon} - \alpha$ (fixing β, γ=0) was a bad fit, since intercepts (α) were close to 0 (**Fig. 4a**).

By fixing γ and α to 0 in **equation (1),** we obtained the Divisive Inhibition (DI) model. In this form, β can be thought of as I/E ratio. Increasing β decreases the observed response ($\boldsymbol{\theta}$) (**Fig. 4a**).

$$\boldsymbol{\theta} = \boldsymbol{\varepsilon} - \beta\boldsymbol{\varepsilon} \qquad (\mathbf{2})$$

Similarly, β was fixed to 1 and α to 0 to get the Divisive Normalization (DN) model. This form of the equation was inspired by the analogous canonical divisive normalization equation for firing

bioRxiv preprint doi: https://doi.org/10.1101/190298; this version posted October 25, 2018. The copyright holder for this preprint (which was not certified by peer review) is the author/funder, who has granted bioRxiv a license to display the preprint in perpetuity. It is made available under aCC-BY-NC-ND 4.0 International license.

rates(Carandini & Heeger, 2012). Here, decrease in γ implies increase in normalization (**Fig. 4a**).

$$\boldsymbol{\theta} = \boldsymbol{\varepsilon} - \frac{\boldsymbol{\varepsilon}}{\gamma + \boldsymbol{\varepsilon}}\boldsymbol{\varepsilon} = \frac{\gamma\boldsymbol{\varepsilon}}{\gamma + \boldsymbol{\varepsilon}} \quad (3)$$

We used least-squares polynomial regression to fit DI and DN models to our data. The goodness of fit for all cells was tested by comparing BIC (Bayesian Information Criterion) (**Fig. 4c**) and reduced chi-squares of the models (**Supplementary Fig. S5o, Methods**). DN (α = 0, β = 1) was better than DI (α = 0, γ = 0) model in explaining the data (BIC: Two-tailed paired t-test, P< 0.00005, reduced chi-square: Two-tailed paired t-test, P< 0.00005, n = 32 cells).

Subthreshold Divisive Normalization (SDN) can be clearly seen in **Figure 4b**, where observed responses to stimuli with 5 mV and 15 mV expected responses are very similar. This shows that SDN allows CA1 cells to integrate a large range of inputs before reaching spike threshold. Thus, testing with a larger range of inputs showed that the initial finding of constant I/E ratios from **Figure 2** needed to be elaborated based on the observed response saturation with increasing input strength. We examine mechanisms for this below (**Fig.5, 6**). In summary, we observed SDN as an outcome of integration of precisely balanced inputs in the CA3-CA1 network.

bioRxiv preprint doi: https://doi.org/10.1101/190298; this version posted October 25, 2018. The copyright holder for this preprint (which was not certified by peer review) is the author/funder, who has granted bioRxiv a license to display the preprint in perpetuity. It is made available under aCC-BY-NC-ND 4.0 International license.

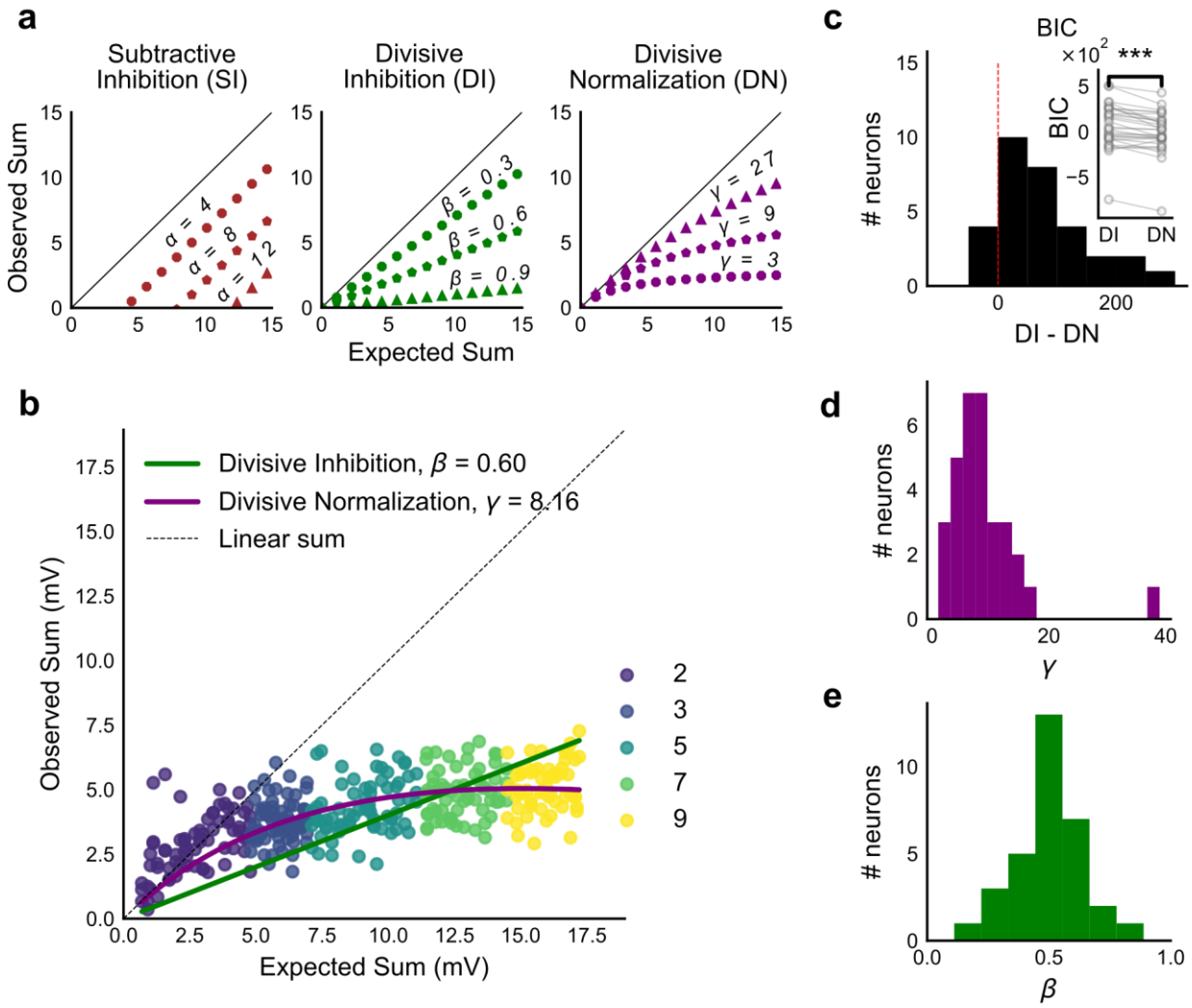

Figure 4: Over a wide input range, integration of CA3 excitatory and feed-forward inhibitory input leads to SDN at CA1

(**a**) Three models of how inhibition interacts with excitation and modulates membrane potential: (left to right) Subtractive Inhibition (SI), Divisive Inhibition (DI) and Divisive Normalization (DN). Note how parameters α, β and γ from **equation (**1**)** affect response output.

(**b**) Divisive normalization seen in a cell stimulated with 2, 3, 5, 7 and 9 square combinations. DN and DI model fits are shown in purple and green respectively.

(**c**) Difference in Bayesian Information Criterion (BIC) values for the 2 models - DI and DN. Most differences between BIC for DI and DN were less than 0, which implied that DN model fit better,

bioRxiv preprint doi: https://doi.org/10.1101/190298; this version posted October 25, 2018. The copyright holder for this preprint (which was not certified by peer review) is the author/funder, who has granted bioRxiv a license to display the preprint in perpetuity. It is made available under aCC-BY-NC-ND 4.0 International license.

accounting for the number of variables used. Insets show raw BIC values. Raw BIC values were consistently lower for DN model, indicating better fit (Two-tailed paired t-test, $P < 0.00005$, n = 32 cells).

(**d**) Distribution of the parameter γ of the DN fit for all cells (median = 7.9, n = 32 cells). Compare with **a**, **b** to observe the extent of normalization.

(**e**) Distribution of the parameter beta of the DI fit for all cells (mean = 0.5, n = 32 cells). Values are less than 1, indicating sublinear behaviour.

CA3 feedforward inhibition is necessary for SDN

We first verified our hypothesis that SDN results from feedforward inhibition in the CA3-CA1 network, and not from intrinsic properties of the CA1 neuron. We thus blocked inhibition and repeated the above experiment. We expected that SDN would be lost and linearity would be reinstated upon blocking inhibition.

We recorded responses of CA1 cells to our array of optical stimuli (**Fig. 1d, 5a**), then applied GABAzine to the bath and repeated the stimulus array (**Fig. 5b**). We found that when inhibition was blocked, summation approached linearity (**Fig. 5b, c**). We compared the scaling parameter γ of the divisive normalization model fit, for the above two conditions (**equation (3)**). The values of γ were larger with inhibition blocked, indicative of approach to linearity (Wilcoxon rank-sum test, $P<0.05$, n = 8 cells) (**Fig. 5c**). While inhibition accounted in large part for the observed sublinear summation, the cells with inhibition blocked showed some residual sublinearity at high stimulus levels, which has been previously attributed to I_A conductance in CA1 neurons(Cash & Yuste, 1999). Based on the conductance equation (**equation (5)**), leak conductance also contributes in part to the residual sublinearity (**Supplementary equation (6)**). Thus, we confirmed that blocking inhibition reduced sublinearity, attenuating SDN.

bioRxiv preprint doi: https://doi.org/10.1101/190298; this version posted October 25, 2018. The copyright holder for this preprint (which was not certified by peer review) is the author/funder, who has granted bioRxiv a license to display the preprint in perpetuity. It is made available under aCC-BY-NC-ND 4.0 International license.

Precise balance is also seen at resting membrane potential

Then, we hypothesised that the membrane potential change evoked by inhibitory synaptic currents could be increasing non-linearly with increasing CA3 input, even though the I/E ratio of conductances would be consistent across the range of input strengths. To address this, we compared responses to identical patterns before and after GABAzine application. For a given cell, for each pattern, we subtracted the initial control response with inhibition intact from the corresponding response with inhibition blocked. This gave us the inhibitory component or 'derived inhibition' for each stimulus pattern (**Fig. 5d, inset**). We found that all stimuli to a cell evoked proportional excitation and inhibition even when recorded at resting potential (**Fig. 5d, e**). Thus, we rejected our hypothesis of non-linear increase in inhibitory post-synaptic potential (IPSP) with excitatory post-synaptic potential at resting membrane potential (EPSP). Over the population, the median slope of the proportionality line was around 0.7, indicating that the EI balance was slightly tilted towards higher excitation than inhibition (**Fig 5f**). IPSP/EPSP ratios (**Fig. 5f**) were smaller than IPSC/EPSC ratios (**Fig. 2d**) due to proximity of inhibition to its reversal (~-70mV), than excitation to its reversal (~0mV), at resting membrane potential (~-65mV). Overall, we saw precise balance in evoked excitatory and inhibitory synaptic potentials for >100 combinations per neuron.

bioRxiv preprint doi: https://doi.org/10.1101/190298; this version posted October 25, 2018. The copyright holder for this preprint (which was not certified by peer review) is the author/funder, who has granted bioRxiv a license to display the preprint in perpetuity. It is made available under aCC-BY-NC-ND 4.0 International license.

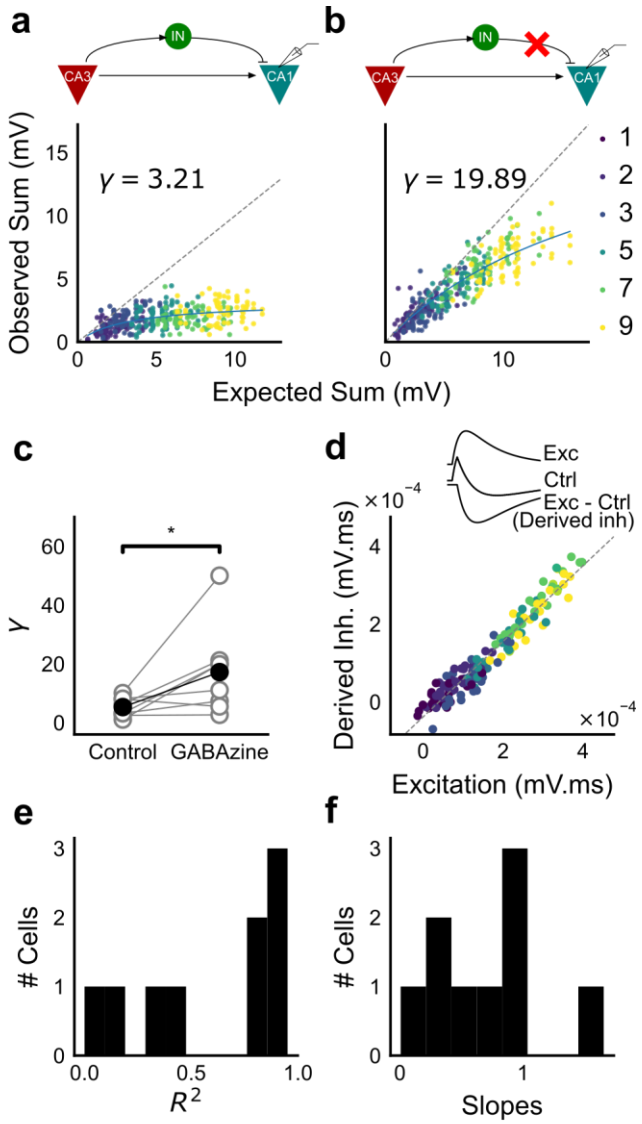

Figure 5: Blocking balanced inhibition at resting membrane potential attenuates SDN

(**a**) Top, schematic of experiment condition. Bottom, a cell showing divisive normalization in control condition.

(**b**) Top, schematic of experiment condition with feedforward inhibition blocked (2uM GABAzine). Bottom, responses of the same cell with inhibition blocked. The responses are much closer to the linear summation line (dashed). The blue lines in **a**, **b** are the fits of the DN model. The value of *γ* of the fit increases when inhibition is blocked.

(**c**) Parameter *γ* was larger with GABAzine in bath (Wilcoxon rank sum test, P<0.05, n = 8 cells), implying reduction in normalization with inhibition blocked.

(**d**) Excitation versus derived inhibition for all points for the cell shown in **a** (area under the curve) (Slope = 0.97, r-square = 0.93, x-intercept = 3.75e-5 mV.ms). Proportionality was seen for all responses at resting

bioRxiv preprint doi: https://doi.org/10.1101/190298; this version posted October 25, 2018. The copyright holder for this preprint (which was not certified by peer review) is the author/funder, who has granted bioRxiv a license to display the preprint in perpetuity. It is made available under aCC-BY-NC-ND 4.0 International license.

membrane potential. Top, 'Derived inhibition' was calculated by subtracting control PSP from the excitatory (GABAzine) PSP for each stimulus combination.

(**e,f**) R^2 (median = 0.8) and slope values (median = 0.7) for all cells (n = 8 cells), showing tight IPSP/EPSP proportionality, and slightly more excitation than inhibition at resting membrane potentials.

Advancing inhibitory onset with increasing input explains SDN

We made a single compartment conductance model (**Fig. 6a, equation (5)**) to analyze the mechanism of SDN. We fit a function of difference of exponentials (**Methods**) to our voltage clamp data to extract the peak amplitudes and kinetics of excitation and inhibition currents (**Methods**). We used these and other parameters from literature (**Supplementary Table 1 and 2**), and constrained the model to have EI balance, i.e. have maximum excitatory (g_{exc}) and inhibitory conductance (g_{inh}) proportional to each other, with a given I/E ratio. To test for SDN, we simulated our model in the range of experimentally determined I/E ratios, ranging from 1-6.

We observed that EI balance with constant EI delay led to a slightly sublinear response which can be approximated with a divisive inhibition model (**Fig. 6b**). In contrast, subthreshold divisive normalization (SDN) implies progressively smaller changes in peak PSP amplitude with increase in excitatory input. We surmised that without changing EI balance, SDN should result if the inhibitory onset delays were an inverse function of the excitation (**Fig. 6e**, **equation (4)**). Hence, we simulated the model with different values of inhibitory delay (δ_{inh}) as a function of the excitation.

$$\delta_{\mathrm{inh}} = \delta_{\mathrm{min}} + me^{-kg_{\mathrm{exc}}} \qquad (4)$$

Here $\delta_{\mathrm{min}}$is the minimum synaptic delay between excitation and inhibition, k sets the steepness of the delay change with excitation, and *m* determines the maximum synaptic delay.

bioRxiv preprint doi: https://doi.org/10.1101/190298; this version posted October 25, 2018. The copyright holder for this preprint (which was not certified by peer review) is the author/funder, who has granted bioRxiv a license to display the preprint in perpetuity. It is made available under aCC-BY-NC-ND 4.0 International license.

In **Fig. 6c**, we show that SDN emerged when we incorporated delays changing as a function of the total excitatory input to the model neuron.

We then tested this model prediction. From the EPSC and IPSC curves (**Methods**), we extracted excitatory and inhibitory onsets, and subtracted the average inhibitory onsets from average excitatory onsets to get inhibitory delay (δ_{inh}) for each stimulus combination. We saw that δ_{inh} indeed varied inversely with total excitation (g_{exc}) (**Fig. 6f, g**). Notably, the relationship of delay with conductance with data from all cells pooled, seems to be a single inverse function, and might be a network property (**Fig.6g, Supplementary Fig. S6c**). This input dependent change in inhibitory delay could be attributed to delayed spiking of interneurons with small excitatory inputs, and quicker firing with larger excitatory inputs. We further illustrate that this delay function emerges naturally by simply applying a threshold to the rising curve of an EPSP at an interneuron (**Supplementary Fig. S6f**). Thus, inhibition clamps down the rising EPSP at progressively earlier times, resulting in saturation of PSP amplitude when excitation is increased (**Fig. 6c,d, Fig. 8**). In **Figure 8a** and **b**, we show using a schematic, how SDN emerges when inhibitory onset changes as an inverse function of input strength.

We then examined the sensitivity of SDN to EI balance and delay (δ_{inh}) between excitation and inhibition. To test if balance and predicted inhibitory delay relationship are required for SDN, we shuffled the balanced g_{inh} in relation with g_{exc}, and separately shuffled the relationship of δ_{inh} and g_{exc}. In both cases, SDN was strongly attenuated, implying that both EI balance and inverse scaling of inhibitory delay were necessary for SDN (**Supplementary Fig. S6 a,b, Supplementary equation (6) to (8)**). Further, we transformed the membrane current equation (**equation(5)**) into the form which resembles divisive normalization equation

bioRxiv preprint doi: https://doi.org/10.1101/190298; this version posted October 25, 2018. The copyright holder for this preprint (which was not certified by peer review) is the author/funder, who has granted bioRxiv a license to display the preprint in perpetuity. It is made available under aCC-BY-NC-ND 4.0 International license.

(**Supplementary Note 1**),and saw that in this form, γ depends on the intrinsic properties of the neuron, and is modulated by delays and EI ratios .

We also observed that we were able to capture the initial linear regime observed in **Fig. 4b** by using the inverse relationship of delay with excitation in this conductance model. This can be understood as follows: At small excitatory input amplitudes, the EI delay is so large that inhibition begins after the peak depolarization of the neuron. The initial linear zone in **Figure 4b** therefore arises when cells receive their normalizing input too late to affect their peak EPSP. At higher stimulus amplitudes the output response is subjected to earlier, and hence increasingly effective inhibition, thus flattening the output curve (**Supplementary Note 1**, **Fig S4a**, **Fig .6c**).

Thus our analysis of a conductance model suggests that SDN could be a general property of balanced feedforward networks, due to two characteristic features: EI balance and inhibitory kinetics. Each of these variables may be subject to plasticity and modulation to attain different amounts of normalization (**Fig. 8c,d, Supplementary Fig.S7**).

bioRxiv preprint doi: https://doi.org/10.1101/190298; this version posted October 25, 2018. The copyright holder for this preprint (which was not certified by peer review) is the author/funder, who has granted bioRxiv a license to display the preprint in perpetuity. It is made available under aCC-BY-NC-ND 4.0 International license.

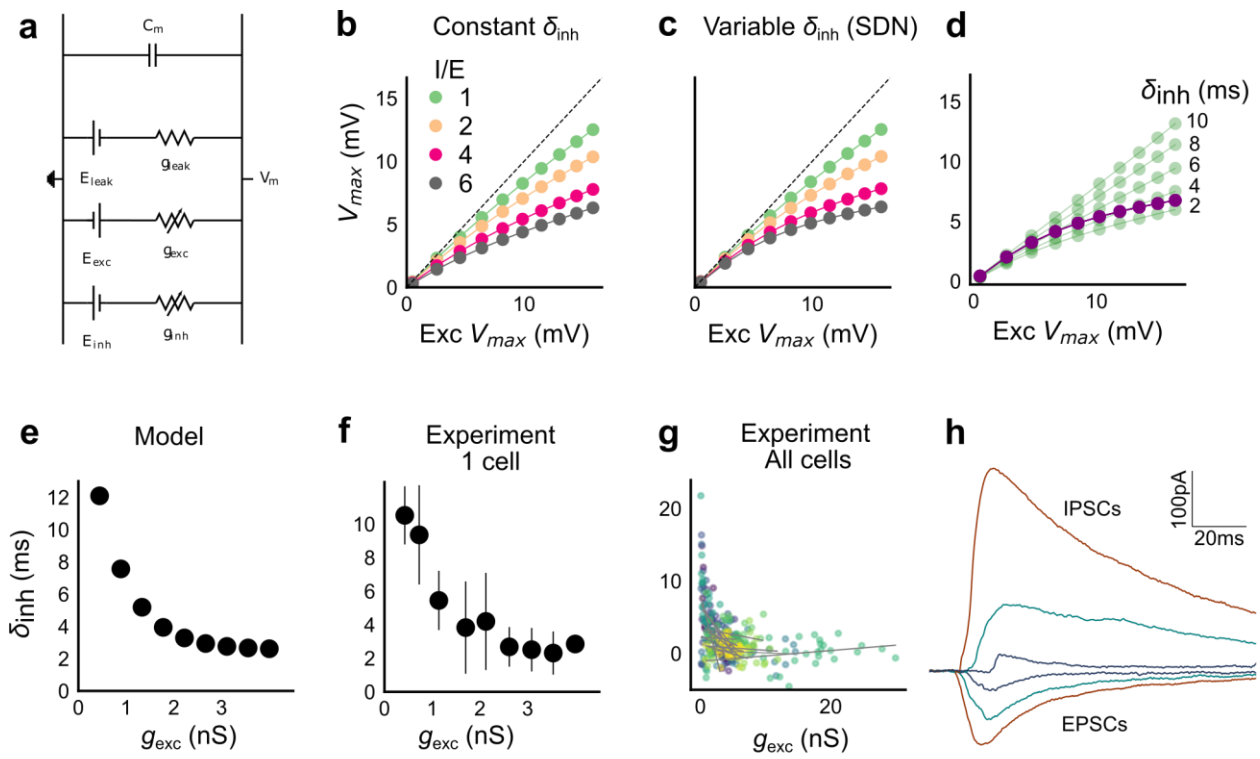

Figure 6: Conductance model predicts Excitatory-Inhibitory delay as an important parameter for divisive normalization.

(**a**) Equivalent circuit for the conductance model showing capacitive, excitatory, inhibitory, and leak components.

(**b**) PSP peak amplitude with both excitatory and balanced inhibitory inputs is plotted against the EPSP peak amplitude with only excitatory input. Model showed sublinear behavior for I/E proportionality ranging from 1 to 6 when the inhibitory delay was kept constant. Different colours show I/E ratios.

(**c**) Same as in **b**, except the inhibitory delay was varied inversely with excitatory conductance (as shown in **e)**. Initial linear zone and saturation of PSPs at higher amplitudes, indicative of SDN were observed, and the normalization gain was sensitive to the I/E ratio. δ_{min} = 2 ms, k = 0.5 nS^{-1}, and m = 8.15 ms.

(**d**) Effect of changing EI delay, keeping I/E ratio constant (I/E ratio = 5). Divisive inhibition (green) seen while changing EI delay values from 2 to 10ms. Divisive normalization (purple) emerges if delays are changed as shown in **e**. δ_{min} = 2 ms, k = 0.5 nS^{-1}, and m = 8.15 ms.

(**e**) Inverse relationship of EI delays with excitation. Inhibitory delay was varied with excitatory conductance in **equation (4)** withδ_{min} = 2 ms, k = 2 nS^{-1}, and m = 13 ms.

(**f**) Data from an example cell showing the relationship of EI delays with excitation. The relationship is similar to the prediction in **e**. Points are binned averages. Error bars are s.d.

(**g**) Data from all cells showing delay as a function of excitation. Different colours indicate different cells (n = 13 cells). Grey lines are linear regression lines through individual cells.

(**h**) Traces showing the decreasing EI delay with increasing amplitude of PSCs. Each trace is an average of 6 repeats.

bioRxiv preprint doi: https://doi.org/10.1101/190298; this version posted October 25, 2018. The copyright holder for this preprint (which was not certified by peer review) is the author/funder, who has granted bioRxiv a license to display the preprint in perpetuity. It is made available under aCC-BY-NC-ND 4.0 International license.

Stimulus information is encoded both in amplitude and time

We next asked if the temporally advancing inhibition (**Fig. 6e-h**) affected PSP peak time with increase in stimulus strength. We calculated the slope of the PSP peak times against the expected axis in the presence (Control) and absence of inhibition (GABAzine) for a given cell. If inhibition cut into excitation and resulted in advancing of peak times with increasing stimulus strength, the slope of peak times would be negative, as shown in **Figure 7a**. Conversely, when inhibition is blocked, slope of peak times is not expected to change much. We saw that for all cells, slope of the peak time with inhibition intact was lower than the slope in the case with inhibition blocked (**Fig. 7b**) (Wilcoxon Rank sum test (P = 0.006), n = 8 cells).

What does SDN mean for information transmission in balanced networks? While SDN allowed the cell to integrate a large range of inputs before reaching spiking threshold, it also resulted in saturation of PSP peaks at larger inputs (**Fig. 4b**). This implied that information about the input was partially 'lost' from the PSP amplitude. . However, PSP times to peak became shorter (**Fig. 7a,b**), hence potentially encoding some information about the input in this time variable (**Fig 7e**, **Fig. 8b**). In contrast, while the peak amplitudes seen with GABAzine predicted the input more reliably, peak times of EPSPs did not change much with input (**Fig. 7b,e**). Thus, PSP peak time may carry additional information about stimulus strength, when EI balance is maintained.

We quantified this using an information theoretical framework(Shannon, 1948).We took linear sum of 1-square PSP peak amplitudes (Expected sum), as a proxy for input strength. We then calculated the mutual information between Expected sum and peak PSP amplitudes of the corresponding N-squares, and between Expected sum and PSP peak timing (**Methods**). Using this, we asked, how is the information about the input divided between PSP peak amplitude and timing? The total mutual information of both peak amplitude and peak timing with expected sum was slightly lesser in the presence of inhibition, but this difference was statistically not significant (**Fig. 7d**) (Wilcoxon Rank sum test (< 0.05), P = 0.11, n = 7 cells). We found that peak timing

bioRxiv preprint doi: https://doi.org/10.1101/190298; this version posted October 25, 2018. The copyright holder for this preprint (which was not certified by peer review) is the author/funder, who has granted bioRxiv a license to display the preprint in perpetuity. It is made available under aCC-BY-NC-ND 4.0 International license.

had more information in presence of inhibition (control), and peak amplitude had more information in absence of inhibition (GABAzine)(Wilcoxon Rank sum test (< 0.05), n = 7 cells) (**Fig. 7e**). Further, we asked, how better can we predict the input, with the knowledge of peak timing, when the peak amplitude is already known? We found that in the presence of inhibition, peak amplitude carried only a part of the total information about the input, and further knowledge of peak time substantially increased the total information. In contrast, in the absence of inhibition, peak amplitude carried most of the information about input, and there was very little gain in information with the knowledge of peak times (**Fig. 7e**) (Wilcoxon Rank sum test (= 0.05), n = 6 cells).

Overall, these results suggest that with inhibition intact, input information is shared between amplitude and time, and knowledge of peak time and amplitude together contains more information about input than either of them alone.

bioRxiv preprint doi: https://doi.org/10.1101/190298; this version posted October 25, 2018. The copyright holder for this preprint (which was not certified by peer review) is the author/funder, who has granted bioRxiv a license to display the preprint in perpetuity. It is made available under aCC-BY-NC-ND 4.0 International license.

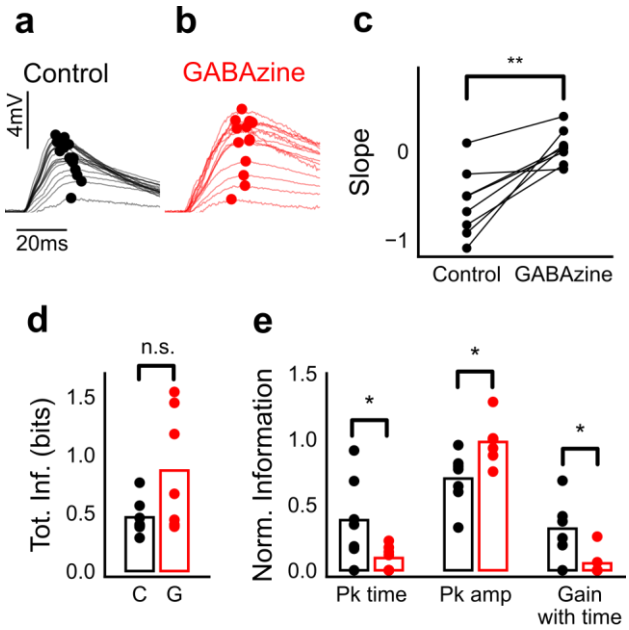

Figure 7: Advancing inhibitory onset changes PSP peak time with increase in stimulus strength

(**a,b**) The PSP peak arrived earlier following larger input in the control case (black), but not with GABAzine in bath (red). Traces for an example cell, binned (20 bins for Expected sum axis) and averaged, for control (black) and with GABAzine in bath (red).

(**c**) Slope of the peak time was more negative in presence of inhibition (control) than when inhibition was blocked (GABAzine) (n = 8 cells).

(**d**) Total mutual information of peak amplitude and peak timing with expected sum was not significantly different between Control and GABAzine case (Wilcoxon Rank sum test (< 0.05), P = 0.11, n = 7 CA1 cells).

(**e**) Normalized mutual information between Expected Vm and peak time, Expected Vm and peak amplitude, and conditional mutual information between Expected Vm and peak time, given the knowledge of peak amplitude. Normalized information was calculated by dividing mutual information by total information (**d**) for each cell. Peak times carried more information in the presence of inhibition, and peak amplitudes carried more information in the absence of inhibition. There was higher gain in information about the input with timing if the inhibition was kept intact (Wilcoxon Rank sum test (P< 0.05), n = 7 (Pk time, Pk amp) and (P= 0.05) n = 6 (Gain with time) CA1 cells).

Modulation of gating with SDN

We next asked how the two basic parameters - I/E ratio and EI delay - modulated the degree of normalization and kinetics of the of SDN curve (**Figure 8 c,d**). Using our conductance model, we measured the normalization parameter γ ($\alpha = 0$, $\beta = 1$, **equation (1)**) for a range of

bioRxiv preprint doi: https://doi.org/10.1101/190298; this version posted October 25, 2018. The copyright holder for this preprint (which was not certified by peer review) is the author/funder, who has granted bioRxiv a license to display the preprint in perpetuity. It is made available under aCC-BY-NC-ND 4.0 International license.

values of I/E ratio and delays, and found that normalization increased systematically with increase in I/E ratio as well as with increase in the steepness of the EI delay relationship (**Figure 8c**). This implies that the degree of normalization of not only an entire neuron, but subsets of inputs to a neuron, could be dynamically altered by changing these parameters. In terms of gating, for a neuron with all inputs tightly balanced, any subset of inputs with reduction in I/E ratio will be gated 'on', corresponding to a condition of higher γ. Neurons can thus differentially gate and respond to specific inputs, while still retaining the capacity to respond to other input combinations.

bioRxiv preprint doi: https://doi.org/10.1101/190298; this version posted October 25, 2018. The copyright holder for this preprint (which was not certified by peer review) is the author/funder, who has granted bioRxiv a license to display the preprint in perpetuity. It is made available under aCC-BY-NC-ND 4.0 International license.

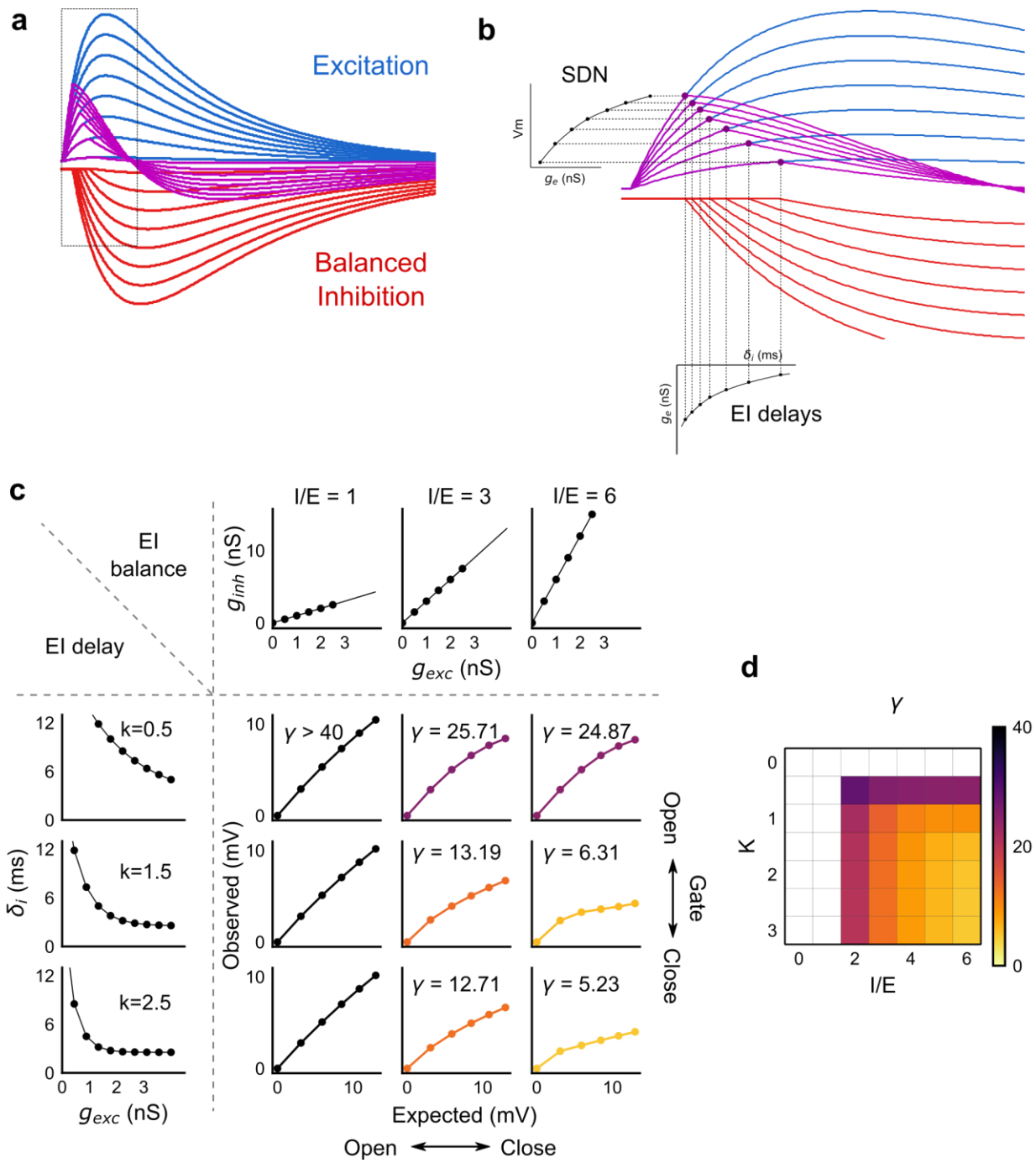

Figure 8: Emergence of SDN from balanced excitation and inhibition, coupled with dynamic EI delays

(**a**) Schematic showing precisely balanced EPSPs (blue) and corresponding IPSPs (red) summing to produce PSPs (purple). The EPSPs and IPSPs increase in equal input steps.

(**b**) Zooming into the portion in the rectangle in **a**. Excitation onset is constant, but inhibition onset changes as an inverse function of input or conductance (g_{exc}), as shown in **Figure 6e**. With increasing input, inhibition arrives earlier and cuts into excitation earlier for each input step. This results in smaller differences in excitatory peaks with each input step, resulting in SDN. The timing of PSP peaks (purple)

bioRxiv preprint doi: https://doi.org/10.1101/190298; this version posted October 25, 2018. The copyright holder for this preprint (which was not certified by peer review) is the author/funder, who has granted bioRxiv a license to display the preprint in perpetuity. It is made available under aCC-BY-NC-ND 4.0 International license.

becomes progressively advanced, whereas the timing of EPSP peaks (blue) does not, consistent with our results in **Figure 7**.

(**c,d**) Normalization as a function of the two building blocks – EI balance (I/E ratio) and EI delays (interneuron recruitment kinetics, k), as predicted by the model. Larger values of both imply greater normalization and increased gating. Colors of the SDN curves depict the value of gamma (*γ*), as shown in the phase plot in **d**. White squares are values of *γ* larger than 40, where almost no normalization occurs.

DISCUSSION

This study describes two fundamental properties of the CA3-CA1 feedforward circuit: balanced excitation and inhibition from arbitrary presynaptic CA3 subsets, and an inverse relationship of excitatory-inhibitory delays with CA3 input amplitude. We used optogenetic photostimulation of CA3 with hundreds of unique stimulus combinations and observed precise EI balance at individual CA1 neurons for every input combination. Stronger stimuli from CA3 led to proportional increase in excitatory and inhibitory amplitudes at CA1, and a decrease in the delay with which inhibition arrived. Consequently, larger CA3 inputs had shorter inhibitory delays, which led to progressively smaller changes in CA1 membrane potential. We term this gain control mechanism subthreshold divisive normalization (SDN). This reduction in inhibitory delay with stronger inputs contributes to a division of input strength coding between PSP amplitude and PSP timing.

Precise balance in the hippocampus

Our findings demonstrate that precise EI balance is maintained by arbitrary combinations of neurons in the presynaptic network, despite the reduced nature of the slice preparation, with no intrinsic network dynamics. This reveals exceptional structure in the connectivity of the network. Theoretical analyses suggest that networks can achieve detailed balance with inhibitory Spike Timing Dependent Plasticity (iSTDP) rules(Hennequin et al., 2017; Luz & Shamir, 2012; T P Vogels, Sprekeler, Zenke, Clopath, & Gerstner, 2011). Such an iSTDP

bioRxiv preprint doi: https://doi.org/10.1101/190298; this version posted October 25, 2018. The copyright holder for this preprint (which was not certified by peer review) is the author/funder, who has granted bioRxiv a license to display the preprint in perpetuity. It is made available under aCC-BY-NC-ND 4.0 International license.

rule has been observed in the auditory cortex(D'amour & Froemke, 2015). Given that balance needs to be actively maintained(Xue, Atallah, & Scanziani, 2014), we suspect that similar plasticity rules(Hennequin et al., 2017) may also exist in the hippocampus.

Precisely balanced networks, with all input subsets balanced, are well suited for input gating (Barron, Vogels, Behrens, & Ramaswami, 2017; Hennequin et al., 2017). The finding that most CA1 cells can be converted to place cells for any arbitrary location predicts the existence of an input gating mechanism (Lee, Lin, & Lee, 2012), but the nature of this mechanism remains unknown. One prediction of precise balance is that inputs for multiple potential place fields may be balanced, and hence place field activity is gated 'off'. Evoked depolarizations(Lee et al., 2012) or dendritic plateau potentials(Bittner et al., 2015; Bittner, Milstein, Grienberger, Romani, & Magee, 2017), which potentiate the subset of active synapses, i.e. change I/E ratio(Grienberger, Milstein, Bittner, Romani, & Magee, 2017), can flip the gate 'on', thereby converting a silent cell to a place cell for that specific place field. This reasoning corroborates the observation of homogenous inhibition suppressing out-of-field heterogeneously tuned excitation(Grienberger et al., 2017), while providing a finer, synaptic scale view of the gating mechanism.

EI delays and temporal coding

In several EI networks in the brain, inhibition is known to suppress excitation after a short time delay, leaving a "window of opportunity" for spiking to occur(Higley & Contreras, 2006; Pouille & Scanziani, 2001; Wehr & Zador, 2003). We have shown that balanced inhibitory input arrives with a delay modulated by the excitatory input in a feedforward circuit. This inverse relationship of EI delay with excitation has not been explicitly reported, though one study showed a decrease in EI delays with increase in whisker stimulation speed in layer 4 cells.(Heiss, Katz, Ganmor, & Lampl, 2008).We show that modulation of EI delay by excitation helps encode the input information in both amplitude and timing of the PSP (**Fig. 7**). Thus, large

bioRxiv preprint doi: https://doi.org/10.1101/190298; this version posted October 25, 2018. The copyright holder for this preprint (which was not certified by peer review) is the author/funder, who has granted bioRxiv a license to display the preprint in perpetuity. It is made available under aCC-BY-NC-ND 4.0 International license.

inputs could be represented with fewer spikes, while conserving input strength information in spike timing. Similar dual encoding has also been observed in somatosensory cortex (Panzeri, Petersen, Schultz, Lebedev, & Diamond, 2001). In CA1, a classic example of dual coding is theta phase precession(Jensen & Lisman, 2000). In addition, spike times during sharp wave ripples, gamma oscillations and time cell representations are also precise up to ~10ms, which is the range of the dynamic “window of opportunity” we observe. This dynamic window also implies that the neuron can transition from temporal integration mode at small input amplitudes to coincidence detection at large input amplitudes(Gabernet, Jadhav, Feldman, Carandini, & Scanziani, 2005; Higley & Contreras, 2006; Wehr & Zador, 2003).

Subthreshold Divisive Normalization (SDN): a novel gain control mechanism

We have introduced Subthreshold Divisive normalization (SDN) as a novel gain control mechanism arising from EI balance and dynamic EI delays. Our study was uniquely able to observe SDN because of the large range of inputs possible in our experiments(Poirazi et al., 2003). SDN expands the dynamic range of inputs that a neuron can accommodate before reaching spike threshold (**Supplementary Fig.S7b**). This is particularly useful for temporally coding, sparsely spiking neurons like CA1(Ahmed & Mehta, 2009). So far, analogous gain control by divisive normalization has only been observed for firing rates of neurons(Carandini & Heeger, 2012). This implies that the timescales of gain change in DN are averaged over periods of tens of milliseconds, over which rates change. As opposed to this, in SDN, gain of every input is normalized at synaptic (millisecond) timescales. Our results add a layer of subthreshold gain control in single neurons, to the known suprathreshold gain control at the population level in CA1(Pouille, Marin-Burgin, Adesnik, Atallah, & Scanziani, 2009). This two-step gain control implies that the dynamic range of the population may be wider than previously estimated. While most experimental observations of firing rate gain change have been explained by the phenomenological divisive normalization equation, the mechanistic basis for normalization has

bioRxiv preprint doi: https://doi.org/10.1101/190298; this version posted October 25, 2018. The copyright holder for this preprint (which was not certified by peer review) is the author/funder, who has granted bioRxiv a license to display the preprint in perpetuity. It is made available under aCC-BY-NC-ND 4.0 International license.

been unclear. SDN provides a biophysical explanation for phenomenological divisive normalization by connecting EI ratios and delays with gain control.

I/E ratio can be changed by neuromodulation(Froemke, 2015; Froemke, Merzenich, & Schreiner, 2007), by short term plasticity mechanisms(Bartley & Dobrunz, 2015; Klyachko et al., 2006; Tsodyks & Markram, 1997)and by disinhibition(Basu et al., 2016). Although we show that EI delays are input amplitude dependent, they may also be modulated by external signals, or behavioural states such as attention(Kim, Ährlund-Richter, Wang, Deisseroth, & Carlén, 2016)(**Fig. 8c,d**). Such interneuron recruitment based changes have been shown to exist in thalamocortical neurons(Gabernet et al., 2005). Dynamic regulation of EI delay has been theoretically explored in balanced networks(Bruno, 2011; Kremkow et al., 2010) for temporal gating of transient inputs independently by amplitude and time. Thus, temporal gating by EI delays(Kremkow et al., 2010), combined with the amplitude gating by detailed balance(Tim P Vogels & Abbott, 2009) could be a powerful mechanism for gating signals(Kremkow et al., 2010) in the hippocampal feedforward microcircuit.

Several studies point towards the existence of precise EI balance in the cortex(Atallah & Scanziani, 2009; Okun & Lampl, 2008; Wehr & Zador, 2003; Wilent & Contreras, 2005; Zhang et al., 2003; Zhou et al., 2014), and here we have shown it in the hippocampus. We propose that input strength dependent inhibitory delay change may be a general property of feedforward network motifs. Together, these suggest that precisely balanced feedforward networks are elegantly suited for controlling gain, timing and gating at individual neurons in neural circuits.

bioRxiv preprint doi: https://doi.org/10.1101/190298; this version posted October 25, 2018. The copyright holder for this preprint (which was not certified by peer review) is the author/funder, who has granted bioRxiv a license to display the preprint in perpetuity. It is made available under aCC-BY-NC-ND 4.0 International license.

METHODS

Animals

All experimental procedures were approved by the National Centre for Biological Sciences Institutional Animal Ethics Committee (Protocol number USB–19–1/2011), in accordance with the guidelines of the Government of India (animal facility CPCSEA registration number 109/1999/CPCSEA) and equivalent guidelines of the Society for Neuroscience. CA3-cre (*C57BL/6-Tg (Grik4-cre) G32-4Stl/J* mice, Stock number 006474) were obtained from Jackson Laboratories. The animals were housed in a temperature controlled environment with a 14-h light: 10h dark cycle, with *ad libitum* food and water.

Virus injections

21-30 days old male transgenic mice were injected with Lox-ChR2 (AAV5.CAGGS.Flex.ChR2-tdTomato.WPRE.SV40) virus obtained from University of Pennsylvania Vector Core. Injection coordinates used were -2.0mm RC, +/-1.9mm ML, -1.5mm DV. ~300-400nl solution was injected into the CA3 region of left or right hemisphere with brief pressure pulses using Picospritzer-III (Parker-Hannifin, Cleveland, OH, USA). Animals were allowed to recover for at least 4 weeks following surgery.

Slice Preparation

8-6 week (4-8 weeks post virus injection) old mice were anesthetized with halothane and decapitated post cervical dislocation. Hippocampus was dissected out and 350um thick transverse hippocampal slices were prepared. Slices (350 microns) were cut in ice-cold high sucrose ASCF containing (in mM) - 87 NaCl, 2.5 KCl, 1.25 NaH2PO4, 25 NaHCO3, 75 sucrose, 10 glucose, 0.5 CaCl2, 7 MgCl2. For cut slice control experiments, CA3 was removed at this stage. Slices were stored in a holding chamber, in artificial cerebro-spinal fluid (aCSF) containing (in mM) - 124 NaCl, 2.7 KCl, 2 CaCl2, 1.3 MgCl2, 0.4 NaH2PO4, 26 NaHCO3, and 35

bioRxiv preprint doi: https://doi.org/10.1101/190298; this version posted October 25, 2018. The copyright holder for this preprint (which was not certified by peer review) is the author/funder, who has granted bioRxiv a license to display the preprint in perpetuity. It is made available under aCC-BY-NC-ND 4.0 International license.

10 glucose, saturated with 95% O2/5% CO2. After at least an hour of incubation, the slices were transferred to a recording chamber and perfused with aCSF at room temperature.

Electrophysiology

Whole cell recording pipettes of 2-5MO were pulled from thick-walled borosilicate glass on a P-97 Flaming/Brown micropipette puller (Sutter Instrument, Novato, CA). Pipettes were filled with internal solution containing (in mM) 130 K-gluconate, 5 NaCl, 10 HEPES, 1 EGTA, 2 MgCl2, 2 Mg-ATP, 0.5 Na-GTP and 10 Phosphocreatinine, pH adjusted to 7.3, osmolarity ~285mOsm. The membrane potential of CA1 cells was maintained near -65mV, with current injection, if necessary. GABA-A currents were blocked with GABAzine (SR-95531, Sigma) at 2uM concentration for some experiments. Cells were excluded from analysis if the input resistance changed by more than 25% (measured for 15/39 cells) or if membrane voltage changed more than 2.5mV (measured for 39/39 cells, maximum current injected to hold the cell at the same voltage was +/-15 pA) of the initial value. For voltage clamp recordings, the K-gluconate was replaced by equal concentration Cs-gluconate. Cells were voltage clamped at 0mV (close to calculated excitation reversal) and -70mV (calculated inhibition reversal) for IPSC and EPSC recordings respectively. At 0mV a small component of APV sensitive inward current was observed, and was not blocked during recordings. Cells were excluded if series resistance went above 25MO or if it changed more than 30% of the initial value, with mean series resistance being 15.7MO +/- 4.5MO std (n=13). For CA3 current clamp recordings, the cells were excluded if the V_m changed by 5mV of the initial value. For whole-cell recordings, neurons were visualized using infrared microscopy and differential interference contrast (DIC) optics on

bioRxiv preprint doi: https://doi.org/10.1101/190298; this version posted October 25, 2018. The copyright holder for this preprint (which was not certified by peer review) is the author/funder, who has granted bioRxiv a license to display the preprint in perpetuity. It is made available under aCC-BY-NC-ND 4.0 International license.

an upright Olympus BX61WI microscope (Olympus, Japan) fitted with a 40X (Olympus LUMPLFLN, 40XW), 0.8NA water immersion objective.

Data Acquisition

Recordings were acquired on a HEKA EPC10 double plus amplifier (HEKA Electronik, Germany) and filtered 2.9 kHz and digitized at 20 kHz. All analysis was done using custom written software in Python 2.7.12 and MatlabR2012b.

Optical stimulation setup

Optical stimulation was done using DMD (Digital Micromirror Device) based Optoma W316 projector (60Hz refresh rate) with its color wheel removed. Image from the projector was miniaturized using a Nikon 50mm f/1.4D lens and formed at the focal plane of the tube lens, confocal to the sample plane. The white light from the projector was filtered using a blue filter (Edmund Optics, 52532), reflected off of a dichroic mirror (Q495LP, Chroma), integrated into the light path of the Olympus microscope, and focused on sample through a 40X objective. This arrangement covered a circular field of around 200 micron diameter on sample. 2.5 pixels measured 1 micron at sample through the 40X objective. Light intensity, measured using a power meter, was about 150mW/mm^2 at sample surface. Background light from black screen usually elicited no or very little synaptic response at recorded CA1 cells. A shutter (NS15B, Uniblitz) was present in the optical path to prevent the slice from being stimulated by background light during the inter-trial interval. The shutter was used to deliver stimulus of 10-15ms per trial. A photodiode was placed in the optical path after the shutter to record timestamps of the delivered stimuli.

Patterned optical stimulation

Processing 2was used for generating optical patterns. All stimuli were 16 micron squares sub sampled from a grid. 16 micron was chosen since it is close to the size of a CA3 soma. The

bioRxiv preprint doi: https://doi.org/10.1101/190298; this version posted October 25, 2018. The copyright holder for this preprint (which was not certified by peer review) is the author/funder, who has granted bioRxiv a license to display the preprint in perpetuity. It is made available under aCC-BY-NC-ND 4.0 International license.

light intensity and square size were standardized to elicit typically 1 spike per cell per stimulus. The number of spikes varied to some extent based on the expression of ChR2, which varied from cell to cell. The switching of spots from one trial to next, at 3 sec inter trial interval, prevented desensitization of ChR2 over successive trials (**Fig. 1g**). Order of presentation N-square was randomized.

For a patched CA1 cell, the number of connected CA3 neurons stimulated per spot was estimated to be in the range of 1 to a maximum of 50 for responses ranging from 0 to 2mV. These calculations assume a contribution of 0.2mV per synapse(Magee & Cook, 2000) and release probability of ~0.2(Murthy et al., 1997). This number includes responses from passing axons, which could also get stimulated in our preparation.

We did not observe any significant cross stimulation of CA1 cells. CA1 cells were patched and the objective was shifted to the CA3 region of the slice, where the optical patterns were then projected. CA1s showed no response to optical stimulation because (i) Use of CA3-cre line restricted ChR2to CA3 cells, (ii) physical shifting of the objective away from CA1 also made sure that any leaky expression, if present, did not elicit responses. Using a cre-based targeted optogenetic stimulation combined with patterned optical stimulation, we designed an experiment which was both more specific and more effective at exploring a large stimulus space. Unlike electrical stimulation, optical stimulation specifically excited CA3 pyramidal neurons, and hence the recorded inhibition was largely feedforward. We believe this specificity was crucial to the finding that I/E ratios for all stimuli to a cell are conserved. Electrical stimulation does not distinguish between neuronal subclasses, and in particular fails to separate out the inhibitory interneurons. Since a key part of our findings emerged from being able to establish a temporal sequence of activation of interneurons, it was crucial to exclude monosynaptic stimulation of interneurons in the experimental design. Second, patterned optical

bioRxiv preprint doi: https://doi.org/10.1101/190298; this version posted October 25, 2018. The copyright holder for this preprint (which was not certified by peer review) is the author/funder, who has granted bioRxiv a license to display the preprint in perpetuity. It is made available under aCC-BY-NC-ND 4.0 International license.

stimulation allowed us to explore a grid of 225 stimulus points in CA3, thereby obtaining a wide array of stimulus combination with large dynamic range, without compromising on the specificity of stimulation (**Fig. 1**, **Supplementary Fig. 1**).

We used 4 different stimulus grids (**Supplementary Fig. S1**). All squares from a grid were presented individually (in random order) and in a stimulus set - randomly chosen combinations of 2, 3, 5, 7, or 9, with 2 or 3 repeats of each combination. The order of presentation of a given N square combination was randomized from cell to cell.

Data analysis and code availability

Data analysis was done using Python, numpy, scipy, matplotlib and other free libraries. All error bars are standard deviations. All analysis code is available as a free library at (https://github.com/sahilm89/linearity).

Data availability

The data that support the findings of this study are available from the corresponding author upon reasonable request.

Pre-processing

PSPs and PSCs were filtered using a low pass Bessel filter at 2 kHz, and baseline normalized using 100 ms before the optical stimulation time as the baseline period. Period of interest was marked as 100 ms from the beginning of optical stimulation, as it was the typical timescales of PSPs. Timing of optical stimulation was determined using timestamp from a photodiode responding to the light from the projector. Trials were flagged if the PSP in the interest period were indistinguishable from baseline period due to high noise, using a 2 sample

bioRxiv preprint doi: https://doi.org/10.1101/190298; this version posted October 25, 2018. The copyright holder for this preprint (which was not certified by peer review) is the author/funder, who has granted bioRxiv a license to display the preprint in perpetuity. It is made available under aCC-BY-NC-ND 4.0 International license.

KS test (p-value < 0.05). Similarly, action potentials in the interest period were flagged and not analyzed, unless specifically mentioned.

Feature extraction

A total of 4measures were used for analyzing PSPs and PSCs (**Fig. 3c**). These were mean, area under the curve, average and area to peak. This was done to be able to catch differences in integration at different timescales, as suggested by Poirazi et al(Poirazi et al., 2003). Trials from CA1 were mapped back to the grid locations of CA3 stimulation for comparison of Expected and Observed responses. Grid coordinate-wise features were calculated by averaging all trials for a given grid coordinate.

Subthreshold Divisive Normalization model

Different models of synaptic integration: Subtractive Inhibition, Divisive Inhibition, and Divisive Normalization models were obtained by constraining parameters in **Equation (1)**. The models were then fit to the current clamp dataset using lmfit. Reduced chi-squares

bioRxiv preprint doi: https://doi.org/10.1101/190298; this version posted October 25, 2018. The copyright holder for this preprint (which was not certified by peer review) is the author/funder, who has granted bioRxiv a license to display the preprint in perpetuity. It is made available under aCC-BY-NC-ND 4.0 International license.

(**Supplementary Fig.S5o**) and Bayesian Information Criterion (**Fig 4c**) were used to evaluate the goodness of fits of these models to experimental data.

Single compartment model

A single compartment conductance based model was created in Python using sympy and numpy. The model consisted of leak, excitatory and inhibitory synaptic conductances (**equation (5)**, **Fig 6a**) to model the subthreshold responses by the CA1 neurons.

$$C_m \frac{dV_m}{dt} = g_{\text{leak}}(V_m - E_{\text{leak}}) + g_{\text{exc}}(V_m - E_{\text{exc}}) + g_{\text{inh}}(V_m - E_{\text{inh}}) \quad \textbf{(5)}$$

The parameters used for the model were taken directly from data, or literature (**Supplementary Table2**). The synaptic conductances$g_{\text{exc}}(t)$, and $g_{\text{inh}}(t)$ were modeled as difference of exponentials (**equation (6) and (7)**):

$$g_{\text{exc}}(t) = \bar{g}_{\text{exc}} \left(\frac{e^{\left(\frac{-t}{\tau_{\text{decay}}}\right)} - e^{\left(\frac{-t}{\tau_{\text{rise}}}\right)}}{-\left(\frac{\tau_{\text{rise}}}{\tau_{\text{decay}}}\right)^{\frac{\tau_{\text{decay}}}{\tau_{\text{decay}} - \tau_{\text{rise}}}} + \left(\frac{\tau_{\text{rise}}}{\tau_{\text{decay}}}\right)^{\frac{\tau_{\text{rise}}}{\tau_{\text{decay}} - \tau_{\text{rise}}}}} \right) \quad \textbf{(6)}$$

$$g_{\text{inh}}(t) = \bar{g}_{\text{inh}} \left(\frac{e^{\left(\frac{\delta_{\text{inh}} - t}{\tau_{\text{decay}}}\right)} - e^{\left(\frac{\delta_{\text{inh}} - t}{\tau_{\text{rise}}}\right)}}{-\left(\frac{\tau_{\text{rise}}}{\tau_{\text{decay}}}\right)^{\frac{\tau_{\text{decay}}}{\tau_{\text{decay}} - \tau_{\text{rise}}}} + \left(\frac{\tau_{\text{rise}}}{\tau_{\text{decay}}}\right)^{\frac{\tau_{\text{rise}}}{\tau_{\text{decay}} - \tau_{\text{rise}}}}} \right) \quad \textbf{(7)}$$

bioRxiv preprint doi: https://doi.org/10.1101/190298; this version posted October 25, 2018. The copyright holder for this preprint (which was not certified by peer review) is the author/funder, who has granted bioRxiv a license to display the preprint in perpetuity. It is made available under aCC-BY-NC-ND 4.0 International license.

For the divisive normalization case, the inhibitory delays (δ_{inh}) were modelled to be an inverse function of $g_{\text{exc}}(t)$ (**equation (4)**). In other cases, they were assumed to be constant and values were taken from **Supplementary Table 2**.

Fitting data

Voltage clamp data was fit to a difference of exponential functions (**equation (8), Supplementary Fig.S6e**) by a non-linear least squares minimization algorithm using lmfit, a freely available curve fitting library for Python. Using this, we obtained amplitudes ($\overline{g}$), time course (τ_{rise},τ_{decay}) and onset delay from stimulus (δ_{onset}) for both excitatory and inhibitory currents. We then calculated inhibitory onset delay (δ_{inh}) by subtracting onset delayof excitatory from inhibitory traces.

$$g(t) = \overline{g}\left(\frac{e^{\left(\frac{\delta_{\text{onset}}-t}{\tau_{\text{decay}}}\right)} - e^{\left(\frac{\delta_{\text{onset}}-t}{\tau_{\text{rise}}}\right)}}{-\left(\frac{\tau_{\text{rise}}}{\tau_{\text{decay}}}\right)^{\frac{\tau_{\text{decay}}}{\tau_{\text{decay}}-\tau_{\text{rise}}}} + \left(\frac{\tau_{\text{rise}}}{\tau_{\text{decay}}}\right)^{\frac{\tau_{\text{rise}}}{\tau_{\text{decay}}-\tau_{\text{rise}}}}}\right) \quad \textbf{(8)}$$

Onset detection

Onsets were also detected using 3 methods. Since we propose onset delays to be a function of the excitation peak, we avoided onset finding methods such as time to 10% of peak, which rely on peaks of the PSCs. We used threshold based (time at which the PSC crossed a threshold), slope based (time at which the slope of the PSC onset was the steepest) and a running window based methods. In the running window method, we run a short window of 0.5 ms, and found the time point at which distributions of two consecutive windows became

bioRxiv preprint doi: https://doi.org/10.1101/190298; this version posted October 25, 2018. The copyright holder for this preprint (which was not certified by peer review) is the author/funder, who has granted bioRxiv a license to display the preprint in perpetuity. It is made available under aCC-BY-NC-ND 4.0 International license.

dissimilar, using a 2 sample KS test. Ideally, with no input, the noise distribution across two consecutive windows should remain identical. All 3 methods gave qualitatively similar results.

Modeling detailed balanced synapses

Synaptic inputs were modeled as sums of probabilistically activated basal synapses with synaptic strengths taken from a lognormal distribution with shape and scale parameters as given by our one square current clamp data (shape = -0.39, scale = 0.80). The width of the weight distribution was altered by changing the scale parameter. Probabilistic synaptic activation was modeled as a binomial process, with synaptic “release probability” for excitatory and inhibitory inputs set at 0.2 and 0.8 respectively.

Inhibitory inputs were generated with various degrees of correlation to the excitation, by shuffling the excitatory weights in differently sized bins, from 1 to the length of the excitatory weight vector, controlled by a parameter ρ. In this manner, as ρ changed from 1 to 0, excitatory and inhibitory weight vectors changed from paired (detailed balance) to completely unpaired but with identical mean and variance of the weight distributions (global balance).

These synapses could be engaged by delivering stimuli, with the number of synapses per stimulus sampled from a Poisson distribution with mean of 5 synapses per stimulus. The total number of excitatory and inhibitory synaptic inputs engaged by a stimulus were always identical. Each stimulus was repeated 6 times. The resultant means and standard deviations for excitatory and inhibitory inputs were plotted against each other to compare different degrees of correlation. The whole process was repeated 100 times, and correlations and r-squared values were averaged to generate the heatmaps.

Mutual Information calculation

Mutual information was calculated by non-parametric entropy estimation and histogram methods. NPEET (https://github.com/gregversteeg/NPEET) was used for non-parametric estimation of Mutual Information. The relationship between variables was shuffled 500 times to

bioRxiv preprint doi: https://doi.org/10.1101/190298; this version posted October 25, 2018. The copyright holder for this preprint (which was not certified by peer review) is the author/funder, who has granted bioRxiv a license to display the preprint in perpetuity. It is made available under aCC-BY-NC-ND 4.0 International license.

find the significance of the Mutual Information estimate. If the true value of MI was not larger than 90% of the distribution obtained by shuffling, mutual information was assumed to be 0. If the total information about the linear sum of one square responses using both peak amplitude and time could not be established with 90% confidence as described above, the cell was excluded from further analysis. We also used the histogram method to find the mutual information (data not shown), and saw a similar trend. Cells with fewer than 80 trials and less than 2 mV inter-quartile range in the linear sum from one square PSP were excluded from the analysis. The calculated linear sum from one square PSP peak amplitude responses, measured N-square peak amplitudes and time were binned with an equal number of bins. The number of bins were calculated using Sturges' Rule, which selects the number of bins as $1 + 3.3 \log n$, where n is the total number of observations for a given neuron. Bin frequencies were divided by the total number of responses to get the probability of occurrence $p(x)$ of each bin.

Mutual Information was then calculated for all pairs of combinations between linear sum, peak amplitude and time using **equation (9) and (10)**.

bioRxiv preprint doi: https://doi.org/10.1101/190298; this version posted October 25, 2018. The copyright holder for this preprint (which was not certified by peer review) is the author/funder, who has granted bioRxiv a license to display the preprint in perpetuity. It is made available under aCC-BY-NC-ND 4.0 International license.

$$MI(X,Y) = H(X) + H(Y) - H(X,Y) \quad \textbf{(9)}$$

Where Shannon's entropy $H(X)$ for a variable X, is given as:

$$H(X) = \sum_{x \in X} -p(x)\log_2 p(x) \quad \textbf{(10)}$$

Further, conditional mutual Information was calculated to measure gain in information about input (linear sum) by knowledge of peak timing when peak amplitude is already known. It was calculated using **Equation 11**.

$$I\,(X\,;Y|Z) = H\,(X,Z) + H(Y,Z) - H(X,Y,Z) - H(Z) \quad \textbf{(11)}$$

Normalized mutual information was calculated by dividing mutual information between pairs of variables by the total information between all three variables (**Equation 12**).

$$I\,(X;Y,Z) = H\,(Z) + H(X,Y) - H(X,Y,Z) \quad \textbf{(12)}$$

bioRxiv preprint doi: https://doi.org/10.1101/190298; this version posted October 25, 2018. The copyright holder for this preprint (which was not certified by peer review) is the author/funder, who has granted bioRxiv a license to display the preprint in perpetuity. It is made available under aCC-BY-NC-ND 4.0 International license.

REFERENCES

Ahmed, O. J., & Mehta, M. R. (2009). The hippocampal rate code: anatomy, physiology and theory. *Trends in Neurosciences*. http://doi.org/10.1016/j.tins.2009.01.009

Anderson, J. S., Carandini, M., & Ferster, D. (2000). Orientation tuning of input conductance, excitation, and inhibition in cat primary visual cortex. *Journal of Neurophysiology*, *84*(2), 909–926.

Atallah, B. V, & Scanziani, M. (2009). Instantaneous Modulation of Gamma Oscillation Frequency by Balancing Excitation with Inhibition. *Neuron*, *62*(4), 566–577. http://doi.org/10.1016/j.neuron.2009.04.027

Barron, H. C., Vogels, T. P., Behrens, T. E., & Ramaswami, M. (2017). Inhibitory engrams in perception and memory. *Proceedings of the National Academy of Sciences*, *114*(26), 201701812. http://doi.org/10.1073/pnas.1701812114

Bartley, A. F., & Dobrunz, L. E. (2015). Short-term plasticity regulates the excitation/inhibition ratio and the temporal window for spike integration in CA1 pyramidal cells. *European Journal of Neuroscience*, *41*(February), 1402–1415. http://doi.org/10.1111/ejn.12898

Basu, J., Zaremba, J. D., Cheung, S. K., Hitti, F. L., Zemelman, B. V., Losonczy, A., & Siegelbaum, S. A. (2016). Gating of hippocampal activity, plasticity, and memory by entorhinal cortex long-range inhibition. *Science*, *351*(6269), aaa5694-aaa5694. http://doi.org/10.1126/science.aaa5694

Bittner, K. C., Grienberger, C., Vaidya, S. P., Milstein, A. D., Macklin, J. J., Suh, J., … Magee, J. C. (2015). Conjunctive input processing drives feature selectivity in hippocampal CA1 neurons. *Nature Neuroscience*, *18*(8), 1133–1142. http://doi.org/10.1038/nn.4062

Bittner, K. C., Milstein, A. D., Grienberger, C., Romani, S., & Magee, J. C. (2017). Behavioral time scale synaptic plasticity underlies CA1 place fields. *Science*, *357*(6355), 1033–1036. http://doi.org/10.1126/science.aan3846

Bruno, R. M. (2011). Synchrony in sensation. *Current Opinion in Neurobiology*.

bioRxiv preprint doi: https://doi.org/10.1101/190298; this version posted October 25, 2018. The copyright holder for this preprint (which was not certified by peer review) is the author/funder, who has granted bioRxiv a license to display the preprint in perpetuity. It is made available under aCC-BY-NC-ND 4.0 International license.

http://doi.org/10.1016/j.conb.2011.06.003

Carandini, M., & Heeger, D. (2012). Normalization as a canonical neural computation. *Nature Reviews Neuroscience*, (November), 1–12. http://doi.org/10.1038/nrn3136

Cash, S., & Yuste, R. (1999). Linear summation of excitatory inputs by CA1 pyramidal neurons. *Neuron*, *22*(2), 383–394. http://doi.org/10.1016/S0896-6273(00)81098-3

D'amour, J. A., & Froemke, R. C. (2015). Inhibitory and Excitatory Spike-Timing-Dependent Plasticity in the Auditory Cortex. *Neuron*, *86*(2), 514–528. http://doi.org/10.1016/j.neuron.2015.03.014

Denève, S., & Machens, C. K. (2016). Efficient codes and balanced networks. *Nature Neuroscience*, *19*(3), 375–82. http://doi.org/10.1038/nn.4243

Enoki, R., Inoue, M., Hashimoto, Y., Kudo, Y., & Miyakawa, H. (2001). GABAergic control of synaptic summation in hippocampal CA1 pyramidal neurons. *Hippocampus*, *11*(6), 683–9. http://doi.org/10.1002/hipo.1083

Froemke, R. C. (2015). Plasticity of Cortical Excitatory-Inhibitory Balance. *Annual Review of Neuroscience*, *38*(1), 195–219. http://doi.org/10.1146/annurev-neuro-071714-034002

Froemke, R. C., Merzenich, M. M., & Schreiner, C. E. (2007). A synaptic memory trace for cortical receptive field plasticity. *Nature*, *450*(7168), 425–429. http://doi.org/10.1038/nature06289

Gabernet, L., Jadhav, S. P., Feldman, D. E., Carandini, M., & Scanziani, M. (2005). Somatosensory integration controlled by dynamic thalamocortical feed-forward inhibition. *Neuron*, *48*(2), 315–327. http://doi.org/10.1016/j.neuron.2005.09.022

Grienberger, C., Milstein, A. D., Bittner, K. C., Romani, S., & Magee, J. C. (2017). Inhibitory suppression of heterogeneously tuned excitation enhances spatial coding in CA1 place cells. *Nature Neuroscience*, *20*(3), 417–426. http://doi.org/10.1038/nn.4486

Haider, B., Duque, A., Hasenstaub, A. R., & McCormick, D. A. (2006). Neocortical Network Activity In Vivo Is Generated through a Dynamic Balance of Excitation and Inhibition.

bioRxiv preprint doi: https://doi.org/10.1101/190298; this version posted October 25, 2018. The copyright holder for this preprint (which was not certified by peer review) is the author/funder, who has granted bioRxiv a license to display the preprint in perpetuity. It is made available under aCC-BY-NC-ND 4.0 International license.

Journal of Neuroscience, *26*(17).

Heiss, J. E., Katz, Y., Ganmor, E., & Lampl, I. (2008). Shift in the Balance between Excitation and Inhibition during Sensory Adaptation of S1 Neurons. *Journal of Neuroscience*, *28*(49), 13320–13330. http://doi.org/10.1523/JNEUROSCI.2646-08.2008

Hennequin, G., Agnes, E. J., & Vogels, T. P. (2017). Inhibitory Plasticity: Balance, Control, and Codependence. *Annual Review of Neuroscience*, *40*(1), annurev-neuro-072116-031005. http://doi.org/10.1146/annurev-neuro-072116-031005

Higley, M. J., & Contreras, D. (2006). Balanced Excitation and Inhibition Determine Spike Timing during Frequency Adaptation. *Journal of Neuroscience*, *26*(2), 448–457. http://doi.org/10.1523/JNEUROSCI.3506-05.2006

Iascone, D. M., Li, Y., Sumbul, U., Doron, M., Chen, H., Andreu, V., … Polleux, F. (2018). Whole-neuron synaptic mapping reveals local balance between excitatory and inhibitory synapse organization. *bioRxiv*, 395384. http://doi.org/10.1101/395384

Ishizuka, N., Cowan, W. M., & Amaral, D. G. (1995). A quantitative analysis of the dendritic organization of pyramidal cells in the rat hippocampus. *J Comp Neurol*, *362*(April), 17–45. http://doi.org/10.1002/cne.903620103

Ishizuka, N., Weber, J., & Amaral, D. G. (1990). Organization of intrahippocampal projections originating from CA3 pyramidal cells in the rat. *Journal of Comparative Neurology*, *295*(4), 580–623. http://doi.org/10.1002/cne.902950407

Jensen, O., & Lisman, J. E. (2000). Position Reconstruction From an Ensemble of Hippocampal Place Cells: Contribution of Theta Phase Coding. *Journal of Neurophysiology*, *83*(5), 2602–2609. http://doi.org/papers://FAFC0638-5DD4-4A81-A69F-F8A54DFE70C3/Paper/p7641

Kim, H., Ährlund-Richter, S., Wang, X., Deisseroth, K., & Carlén, M. (2016). Prefrontal Parvalbumin Neurons in Control of Attention. *Cell*, *164*(1–2), 208–218. http://doi.org/10.1016/j.cell.2015.11.038

Klyachko, V. A., Stevens, C. F., Zucker, R., Regehr, W., Abbott, L., Regehr, W., … Stevens, C.

bioRxiv preprint doi: https://doi.org/10.1101/190298; this version posted October 25, 2018. The copyright holder for this preprint (which was not certified by peer review) is the author/funder, who has granted bioRxiv a license to display the preprint in perpetuity. It is made available under aCC-BY-NC-ND 4.0 International license.

(2006). Excitatory and Feed-Forward Inhibitory Hippocampal Synapses Work Synergistically as an Adaptive Filter of Natural Spike Trains. *PLoS Biology*, *4*(7), e207. http://doi.org/10.1371/journal.pbio.0040207

Kremkow, J., Aertsen, A., & Kumar, A. (2010). Gating of Signal Propagation in Spiking Neural Networks by Balanced and Correlated Excitation and Inhibition. *Journal of Neuroscience*, *30*(47), 15760–15768. http://doi.org/10.1523/JNEUROSCI.3874-10.2010

Lee, D., Lin, B.-J., & Lee, A. K. (2012). Hippocampal Place Fields Emerge upon Single-Cell Manipulation of Excitability During Behavior. *Science*, *337*(6096), 849–853. http://doi.org/10.1126/science.1221489

Liu, G. (2004). Local structural balance and functional interaction of excitatory and inhibitory synapses in hippocampal dendrites. *Nature Neuroscience*, *7*(4), 373–379. http://doi.org/10.1038/nn1206

Lovett-Barron, M., Turi, G. F., Kaifosh, P., Lee, P. H., Bolze, F., Sun, X.-H., … Losonczy, A. (2012). Regulation of neuronal input transformations by tunable dendritic inhibition. *Nature Neuroscience*, *15*(3), 423–30, S1-3. http://doi.org/10.1038/nn.3024

Luz, Y., & Shamir, M. (2012). Balancing feed-forward excitation and inhibition via hebbian inhibitory synaptic plasticity. *PLoS Computational Biology*, *8*(1). http://doi.org/10.1371/journal.pcbi.1002334

Magee, J. C., & Cook, E. P. (2000). Somatic EPSP amplitude is independent of synapse location in hippocampal pyramidal neurons. *Nature Neuroscience*, *3*(9), 895–903. http://doi.org/10.1038/78800

Murthy, V. N., Sejnowski, T. J., & Stevens, C. F. (1997). Heterogeneous release properties of visualized individual hippocampal synapses. *Neuron*, *18*, 599–612. http://doi.org/10.1016/S0896-6273(00)80301-3

Okun, M., & Lampl, I. (2008). Instantaneous correlation of excitation and inhibition during ongoing and sensory-evoked activities. *Nature Neuroscience*, *11*(5), 535–7.

bioRxiv preprint doi: https://doi.org/10.1101/190298; this version posted October 25, 2018. The copyright holder for this preprint (which was not certified by peer review) is the author/funder, who has granted bioRxiv a license to display the preprint in perpetuity. It is made available under aCC-BY-NC-ND 4.0 International license.

http://doi.org/10.1038/nn.2105

Okun, M., & Lampl, I. (2009). Balance of excitation and inhibition. *Scholarpedia*, *4*(8), 7467. http://doi.org/10.4249/scholarpedia.7467

Panzeri, S., Petersen, R. S., Schultz, S. R., Lebedev, M., & Diamond, M. E. (2001). The role of spike timing in the coding of stimulus location in rat somatosensory cortex. *Neuron*, *29*(3), 769–777. http://doi.org/10.1016/S0896-6273(01)00251-3

Poirazi, P., Brannon, T., & Mel, B. W. (2003). Arithmetic of Subthreshold Synaptic Summation in a Model CA1 Pyramidal Cell. *Neuron*, *37*(6), 977–987. Retrieved from http://www.sciencedirect.com/science/article/pii/S089662730300148X

Pouille, F., Marin-Burgin, A., Adesnik, H., Atallah, B. V., & Scanziani, M. (2009). Input normalization by global feedforward inhibition expands cortical dynamic range. *Nature Neuroscience*, *12*(12), 1577–85. http://doi.org/10.1038/nn.2441

Pouille, F., & Scanziani, M. (2001). Enforcement of temporal fidelity in pyramidal cells by feed-forward somatic inhibition. *Science*, *293*(5532), 325–331. http://doi.org/10.1126/science.1060342

Shannon, C. E. (1948). A Mathematical Theory of Communication. *Bell System Technical Journal*, *27*(3), 379–423. http://doi.org/10.1002/j.1538-7305.1948.tb01338.x

Shu, Y., Hasenstaub, A., Badoual, M., Bal, T., & McCormick, D. A. (2003). Barrages of Synaptic Activity Control the Gain and Sensitivity of Cortical Neurons. *Journal of Neuroscience*, *23*(32).

Tsodyks, M. V., & Markram, H. (1997). The neural code between neocortical pyramidal neurons depends on neurotransmitter release probability. *Proceedings of the National Academy of Sciences*, *94*(2), 719–723. http://doi.org/10.1073/pnas.94.2.719

Vogels, T. P., & Abbott, L. F. (2009). Gating multiple signals through detailed balance of excitation and inhibition in spiking networks. *Nature Neuroscience*, *12*(4), 483–91.

bioRxiv preprint doi: https://doi.org/10.1101/190298; this version posted October 25, 2018. The copyright holder for this preprint (which was not certified by peer review) is the author/funder, who has granted bioRxiv a license to display the preprint in perpetuity. It is made available under aCC-BY-NC-ND 4.0 International license.

http://doi.org/10.1038/nn.2276

Vogels, T. P., Sprekeler, H., Zenke, F., Clopath, C., & Gerstner, W. (2011). Inhibitory plasticity balances excitation and inhibition in sensory pathways and memory networks. *Science (New York, N.Y.)*, *334*(6062), 1569–73. http://doi.org/10.1126/science.1211095

Wehr, M., & Zador, A. M. (2003). Balanced inhibition underlies tuning and sharpens spike timing in auditory cortex. *Nature*, *426*(6965), 442–446. http://doi.org/10.1038/nature02116

Wilent, W. B., & Contreras, D. (2005). Dynamics of excitation and inhibition underlying stimulus selectivity in rat somatosensory cortex. *Nature Neuroscience*, *8*(10), 1364–1370. http://doi.org/10.1038/nn1545

Xue, M., Atallah, B. V., & Scanziani, M. (2014). Equalizing excitation–inhibition ratios across visual cortical neurons. *Nature*, *511*(7511), 596–600. http://doi.org/10.1038/nature13321

Yizhar, O., Fenno, L. E., Prigge, M., Schneider, F., Davidson, T. J., O'Shea, D. J., … Deisseroth, K. (2011). Neocortical excitation/inhibition balance in information processing and social dysfunction. *Nature*, *477*(7363), 171–178. http://doi.org/10.1038/nature10360

Zhang, L. I., Tan, A. Y. Y., Schreiner, C. E., & Merzenich, M. M. (2003). Topography and synaptic shaping of direction selectivity in primary auditory cortex. *Nature*, *424*(6945), 201–205. http://doi.org/10.1038/nature01796

Zhou, M., Liang, F., Xiong, X. R., Li, L., Li, H., Xiao, Z., … Zhang, L. I. (2014). Scaling down of balanced excitation and inhibition by active behavioral states in auditory cortex. *Nature Neuroscience*, *17*(6), 841–850. http://doi.org/10.1038/nn.3701

ACKNOWLEDGEMENTS

AB and SM were supported by NCBS/TIFR and Council of Scientific and Industrial Research (CSIR). We acknowledge support from the University Grants Commission/Israel Science Foundation grant (UGC/ISF No. F 6-18/2014(IC)). We acknowledge the National

bioRxiv preprint doi: https://doi.org/10.1101/190298; this version posted October 25, 2018. The copyright holder for this preprint (which was not certified by peer review) is the author/funder, who has granted bioRxiv a license to display the preprint in perpetuity. It is made available under aCC-BY-NC-ND 4.0 International license.

Mouse Resource (NaMoR) facility funded by Department of Biotechnology for housing and maintaining all animals used in this study. We would like to thank Nikhila Krishnan and Shriya Palchaudhuri for help with genotyping; and Kambadur Ananthamurthy, Sathyaa Subramaniyam, Deepanjanli Dwivedi, Oliver Muthmann, Mehrab Modi, Dinesh Natesan, Aditya Gilra, Arvind Kumar and Rishikesh Narayanan for discussions and suggestions on the manuscript.

AUTHOR CONTRIBUTIONS

AB, SM and USB designed the study. AB performed the experiments and did part of the analysis. SM did most of the analysis and implemented the models. All authors wrote the manuscript.

CONFLICT OF INTEREST

The authors declare that the research was conducted in the absence of any commercial or financial relationships that could be construed as a potential conflict of interest.